An overview of the statistical properties of two-dimensional turbulence in fluids with particles, conducting fluids, fluids with polymer additives, binary-fluid mixtures, and superfluids

Rahul Pandit [iD], Debarghya Banerjee, Akshay Bhatnagar, Marc Brachet [iD], Anupam Gupta [iD], Dhrubaditya Mitra, Nairita Pal, Prasad Perlekar, Samriddhi Sankar Ray [iD], Vishwanath Shukla, and Dario Vincenzi

View Online   Export Citation   CrossMark

ARTICLES YOU MAY BE INTERESTED IN

AIP Publishing

An overview of the statistical properties of two-dimensional turbulence in fluids with particles, conducting fluids, fluids with polymer additives, binary-fluid mixtures, and superfluids

Rahul Pandit,[1,a)] Debarghya Banerjee,[2,b)] Akshay Bhatnagar,[3,c)] Marc Brachet,[4,d)]
Anupam Gupta,[5,e)] Dhrubaditya Mitra,[3,f)] Nairita Pal,[1,g)] Prasad Perlekar,[6,h)]
Samriddhi Sankar Ray,[7,i)] Vishwanath Shukla,[8,j)] and Dario Vincenzi[9,k)]

[1]*Centre for Condensed Matter Theory, Department of Physics, Indian Institute of Science,
Bangalore 560012, India*
[2]*Huygens Laboratory, Niels Bohrweg 2, 2333 CA Leiden, The Netherlands*
[3]*Nordita, KTH Royal Institute of Technology and Stockholm University, Roslagstullsbacken 23,
10691 Stockholm, Sweden*
[4]*Laboratoire de Physique Statistique, École Normale Supérieure, PSL Research University; UPMC Univ
Paris 06, Sorbonne Universités; Université Paris Diderot, Sorbonne Paris-Cité; CNRS, 24 Rue Lhomond,
75005 Paris, France*
[5]*FERMaT, Université de Toulouse, CNRS, INPT, INSA, UPS, Toulouse, France*
[6]*TIFR Centre for Interdisciplinary Sciences, 21 Brundavan Colony, Narsingi, Hyderabad 500075, India*
[7]*International Centre for Theoretical Sciences, TIFR, Survey No. 151, Shivakote, Hesaraghatta Hobli,
Bangalore 560089, India*
[8]*SPEC, CEA, CNRS, Universit Paris-Saclay, CEA Saclay, 91191 Gif-sur-Yvette, France*
[9]*Université Côte d'Azur, CNRS, LJAD, 06108 Nice, France*

We present an overview of the statistical properties of turbulence in two-dimensional (2D) fluids. After a brief recapitulation of well-known results for statistically homogeneous and isotropic 2D fluid turbulence, we give an overview of recent progress in this field for such 2D turbulence in conducting fluids, fluids with polymer additives, binary-fluid mixtures, and superfluids; we also discuss the statistical properties of particles advected by 2D turbulent fluids. *Published by AIP Publishing.*
https://doi.org/10.1063/1.4986802

I. INTRODUCTION

Two-dimensional (2D) fluid turbulence is of central importance not only in fluid dynamics but also in nonequilibrium statistical mechanics. Since the early theoretical studies of Fjørtoft, Kraichnan, Leith, and Batchelor,[1–4] it has been recognized that 2D fluid turbulence is fundamentally different from its three-dimensional (3D) counterpart.[5–8] Perhaps the most striking difference is the following: the fluid-energy spectrum $E(k)$ in forced, statistically steady, homogeneous and isotropic 2D fluid turbulence shows (a) a *forward cascade* of enstrophy (or the mean-square vorticity), from the forcing wave number k_f, at which energy is injected into the fluid, to wave numbers $k > k_f$ and (b) an *inverse cascade* of energy to $k < k_f$, which leads, in the absence of friction, to the formation of large vortices, whose size is comparable to that of the system. Not only is 2D fluid turbulence of theoretical interest but it can also be realized, to a very good approximation, in a variety of experimental flows. These include the following: (1) Geophysical and planetary flows,[9–12] for instance, in the atmosphere, where the thickness of the atmospheric layer is much smaller than its lateral extent, so it is approximately a two-dimensional fluid; illustrative examples include the atmospheric mesoscale[13–16] and large-scale zonal flows in the oceans or in the atmosphere of Jupiter;[17–20] (2) astrophysical flows, such as those in accretion disks;[21–23] (3) laboratory flows in, for instance, soap films, thin layers of electrolytes that can be driven electromagnetically, or Faraday-wave systems.[24–41] Advances in computational resources, which have followed Moore's law for several decades,[42] and new numerical schemes have made it possible to carry out direct numerical simulations (DNSs), with ever increasing resolution and run times, of two-dimensional fluid turbulence;[43–56] such DNSs complement experimental and theoretical investigations in important ways. Different aspects of such investigations have been covered in various reviews[7,8,12,57–61] and books.[5,6,62,63]

The essential statistical properties of 2D fluid turbulence are well known (see, e.g., the summary towards the end of Ref. 7). In contrast to the case of a 3D fluid, there are an infinite number of conserved quantities, in the 2D, inviscid, unforced fluid; the energy and the enstrophy are the most important among these. As a consequence of this, 2D

---

a)Also at Jawaharlal Nehru Centre For Advanced Scientific Research, Jakkur, Bangalore, India. Electronic mail: rahul@physics.iisc.ernet.in.
b)Electronic mail: banerjee@lorentz.leidenuniv.nl
c)Electronic mail: akshayphy@gmail.com
d)Electronic mail: brachet@physique.ens.fr
e)Electronic mail: anupam1509@gmail.com
f)Electronic mail: dhruba.mitra@gmail.com
g)Electronic mail: nairitap2009@gmail.com
h)Electronic mail: perlekar@tifrh.res.in
i)Electronic mail: samriddhisankarray@gmail.com
j)Electronic mail: research.vishwanath@gmail.com
k)Electronic mail: dario.vincenzi@unice.fr

29, 111112-1

fluid turbulence displays, at large Reynolds numbers *Re*, an *inverse cascade* of energy, from the length scale $l_f \sim 2\pi k_f^{-1}$, at which the force acts, to larger length scales, and a *forward cascade* of enstrophy, from l_f to smaller length scales. (Recall, for comparison, that 3D fluid turbulence displays only a forward cascade of energy.[5,6,62]) These two cascades lead to the following power-law forms for the energy spectrum in the inverse- and forward-cascade parts, respectively: $E(k) \sim k^{-5/3}$ and $E(k) \sim k^{-\delta}$, with $\delta = 3$ in the absence of friction; δ increases with the friction coefficient because of nonlocal interactions.[7,53,54,64–66] The dependence of other statistical properties, in the forward-cascade regime, is discussed in Ref. 54; furthermore, velocity structure functions (see below) do not show significant multiscaling, but vorticity structure functions do. Very-high-resolution studies are required to uncover both inverse- and forward-cascade power-law ranges in a single DNS;[53,55] for such ranges in one experiment see, e.g., Ref. 41. In the absence of friction, a very long run is required to obtain a statistically steady state, with two, large coherent vortices (of opposite sign in DNSs that enforce zero mean vorticity), in the inverse-cascade regime.[56] An analysis, based on the stochastic-Loewner evolution, of isolines of the vorticity indicates that, in the inverse-cascade regime, 2D fluid turbulence displays conformal invariance.[67]

Interesting behaviors have also been observed in confined 2D flows, in which the accumulation of energy at the largest scales results in the formation of a large-scale circulation, which exhibits random reversals.[24] Recent experimental[68] and numerical simulation[69] studies have investigated this phenomenon in detail by varying the large-scale friction. The flow states, with random reversals of the large-scale circulation, have a bimodal velocity probability distribution function (PDF) with two symmetric maxima, corresponding to opposite signs of the large-scale circulation. They emerge from bifurcations, over a turbulent background, with Gaussian velocity fields, as the friction is reduced. If the friction is reduced even more, then the reversals of the large-scale circulation become progressively less frequent and, ultimately, may end up in a condensed state, in which most of the kinetic energy is carried by the large-scale circulation. These bifurcations occur within strongly turbulent regimes and are, therefore, less understood than bifurcations from a steady or periodic flow. However, very recently, Ref. 70 has attempted to provide a conceptual framework for treating such reversals, by using the truncated Euler equation to describe the large length scales of the turbulent flow. In particular, it shows that the length scales larger than the forcing scales are in statistical equilibrium; and the PDFs described above can be recovered by using the micro-canonical distribution; transitions are obtained from Gaussian to bimodal distributions and broken-ergodicity. Another related study in Ref. 71 uses the 2D stochastic Navier-Stokes equations to examine the bifurcations in the flow topology; it has reported bistable behavior in this setting, accompanied by random changes from dipoles to unidirectional flows.

We do not dwell on these statistical properties of 2D fluid turbulence in detail because they have been covered in several papers, a fair fraction of which we have cited above. Our goal is to provide an overview of the statistical properties of homogeneous, isotropic 2D turbulence in other hydrodynamical systems, against the backdrop of what we have summarized above for 2D fluid turbulence. The specific systems we study are 2D fluids with particles, conducting fluids, fluids with polymer additives, binary-fluid mixtures, and superfluids. The study of turbulence in these 2D systems is considerably more challenging than its 2D classical-fluid counterpart. In particular, the statistical properties of turbulence in these systems depend on more control parameters than Re and k_f. A systematic exploration of the space of control parameters is often not feasible, with a given level of computational or experimental resources. It is useful to compare studies of these different types of turbulence to bring out similarities between them, where they exist. Furthermore, the study of turbulence in these systems is inherently interdisciplinary, for it requires methods from both fluid mechanics and statistical mechanics. We hope that this overview, which is based principally on our studies of these problems, will bring together experts from both these areas to work on the challenging problems that we discuss here.

There has been a considerable progress in understanding the statistical properties of particle transport by turbulent flows, in general,[72–78] and by 2D turbulent fluids, in particular (see, e.g., Refs. 79–81 and 83–86). It is of relevance to a wide class of problems in many industrial, atmospheric, geophysical, atmospheric, and astrophysical settings.[75,76,78] In recent times, the clustering and preferential concentration of heavy particles in a turbulent flow[72,83,84,87,88] and the statistics of particle-track geometries[85,86,89–91] have attracted considerable attention. We give a brief outline of such studies and then show how particles in a 2D turbulent flow can be used to define (a) a persistence problem[92,93] for such turbulence, (b) quasi-Lagrangian fields,[94] which provide the natural framework for studying the dynamic multiscaling of time-dependent structure functions,[95–100] and (c) various statistical properties for the geometries of particle trajectories.[85,86,89–91] We also give a summary of the statistical properties of elliptical particles in a 2D turbulent flow.[101]

Inverse and forward cascades occur in homogeneous, isotropic, and statistically steady magnetohydrodynamic (MHD) turbulence, in both 3D[102] and 2D, on which we concentrate here. The statistical properties of 2D MHD turbulence, in which there is an inverse cascade of the magnetic vector potential, have attracted considerable attention.[103–117] Recently we have carried out detailed direct numerical simulations (DNSs) of the forced 2D MHD equations, with friction.[115] In this DNS, we obtain spectral regimes with a substantial inverse-cascade region. This allows us to compare the results of DNSs with and without friction both from our study and those prior to it.

The effects of polymer additives on fluid flows have been the subject of several studies, principally in 3D, because of the remarkable phenomena of (a) drag reduction,[118] in wall-bounded turbulent flows, and (b) elastic turbulence or rheochaos (see, e.g., Refs. 119–121) at low Reynolds numbers. In fully developed turbulent flows, which are statistically homogeneous and isotropic, the addition of polymers leads to dissipation reduction, modifies the fluid energy spectrum,

and suppresses structures at small scales.[122–132] The effects of polymer additives on 2D flows have also been studied in experiments[133–135] and DNSs[136–141] of fluid films with polymer additives; we give an overview of some of our recent work here.

Multiphase, turbulent flows occur in several industrial and natural settings;[78] these include particle-laden flows that we have mentioned above. In addition, such flows can have different, coexisting, liquid phases. The simplest examples are binary-fluid mixtures, such as an oil-water mixture, which have been studied extensively in equilibrium and non-equilibrium statistical mechanics to understand phase equilibria and critical phenomena,[143–145] nucleation,[146] spinodal decomposition,[147–150] and the late-stage growth during phase separation (also called coarsening).[148,151–154] It is conventional to refer to minority (low-volume-fraction) and majority (high-volume-fraction) phases; if these phases do not mix, then minority-phase droplets are advected by the background flow of the majority-phase; however, the droplets are not passive, for they affect the flow even as they are affected by it. If the volume fractions of the two phases are equal (a 50-50 mixture), then, in the two-phase regime, the system exhibits phase separation, unless this is suppressed by the turbulent flow of this binary-fluid mixture. Such droplet dynamics or the suppression of phase separation (coarsening arrest) by turbulence are active areas of research both in 3D (see, e.g., Ref. 150 and references therein) or in 2D, on which we concentrate here. In particular, we give an overview of recent studies[155–157] that use the Cahn-Hilliard-Navier-Stokes (CHNS) equations to study such droplet dynamics and coarsening arrest. The Cahn-Hilliard part of these equations uses a scalar field ϕ, called the phase field, to distinguish between the two components of the binary mixture; ϕ changes continuously across interfaces that separate the two phases, so boundary conditions do not have to be enforced on a sharp, moving interface.

Superfluid turbulence is of central importance in understanding the dynamics and nonequilibrium statistical mechanics of quantum fluids.[158–162] Such turbulence has been studied more often in three dimensions (3D) than in two dimensions (2D). As we have noted above, in classical fluids, the statistical properties of turbulence are qualitatively different in 2D and 3D. These differences are being examined now for *superfluid* turbulence. The dynamics of a superfluid can be described at many levels. For example, if we are interested in resolving spatial scales comparable to the healing length of the core of a quantum vortex, then, for a weakly interacting Bose superfluid, at low temperatures, we can use the Gross-Pitaevskii (GP) equation to obtain the spatiotemporal evolution of the superfluid. However, if we consider much larger length scales, then a two-fluid description, with normal and superfluid components, is adequate; the Hall-Vinen-Bekharevich-Khalatnikov (HVBK), two-fluid model,[162–167] is used most often in such cases. We give an overview of our recent studies of both inverse and forward cascades of energy and enstrophy in the 2D HVBK system.[168] To consider the role of quantum vortices in superfluid turbulence, the simplest model we can use is the GP equation. It is important here to study both the thermalization of the Fourier-truncated GP system in 2D and to understand the development of cascades when it is forced and when a term

is added to model dissipation at small spatial scales.[169–180] Furthermore, particles have been used to track quantum vortices in superfluid turbulence.[181] It is natural, therefore, to ask about particle transport by superfluid turbulence. This can be done both at the HVBK level[182] and the level of the GP equation. We give an overview of recent results for the 2D GP system.[174,183]

The remainder of our paper is organized as follows. Section II introduces the equations we use to model the 2D fluid systems we have mentioned above; we also outline the numerical methods that we use to carry out DNSs of these models. In Sec. III, we provide an overview of the results that have been obtained for these models and compare them with experimental results if they are available. Section IV contains a discussion of our results and conclusions.

II. MODELS AND NUMERICAL METHODS

The two-dimensionality of the flows we have mentioned above is the unifying theme of our paper. The statistical properties of turbulence in the two-dimensional (2D) Navier-Stokes (NS) equation are markedly different from their 3D NS counterparts. We cover the statistical properties of homogeneous, isotropic 2D turbulence in other hydrodynamical systems, namely, 2D fluids with particles, conducting fluids, fluids with polymer additives, binary-fluid mixtures, and superfluids. It is useful to study the different models for these systems separately. Therefore, in this section, we define the models that are used to study 2D turbulence in (a) Navier-Stokes fluids (Subsection II A), (b) MHD (Subsection II B), (c) fluids with polymer additives (Subsection II C), (d) binary-fluid mixtures (Subsection II D), (e) superfluids, at the level of the two-fluid HVBK model (Subsection II E), and (f) superfluids, at the level of the GP equation (Subsection II F). We also define various quantities that are useful in characterizing the statistical properties of turbulence in these systems.

A. Navier-Stokes fluid

The forced, incompressible, 2D Navier-Stokes (2D NS) equation, with air-drag-induced friction, can be written most conveniently in the following vorticity ω–stream-function ψ representation, which ensures incompressibility of the fluid (we restrict ourselves to low-Mach-number flows):

$$\partial_t \omega - J(\psi, \omega) = \nu \nabla^2 \omega - \alpha \omega + f^\omega, \tag{1}$$

where $\nabla^2 \psi = \omega$, $J(\psi, \omega) \equiv (\partial_x \psi)(\partial_y \omega) - (\partial_x \omega)(\partial_y \psi)$, and the velocity $\mathbf{u} \equiv (-\partial_y \psi, \partial_x \psi)$; the kinematic viscosity and coefficient of friction are, respectively, ν and α; the uniform density ρ is set to unity; and f^ω is the external force that injects energy at the injection-scale wavenumber k_f. If it is required, we can non-dimensionalize lengths by k_f^{-1}, time by k_f^2/ν, α by $k_f^2 \nu$. This non-dimensionalized friction, the Grashof number (i.e., the non-dimensionalized force) $\mathcal{G} \equiv 2\pi ||f^\omega||^2/(k_f^3)\nu^2)$, where $||f^\omega||^2 \equiv [\int_\mathcal{A} |f^\omega|^2 dx]^{1/2}$ and $\mathcal{A}$ is the area of the film, and the injection scale k_f are the three important control parameters; their values govern the statistical properties of the turbulent, non-equilibrium, but statistically steady, state which the system reaches, typically, but not always, after a few

large-eddy-turnover times $\tau_L = L/u_{rms}$, where L is the linear size of the domain, most often a square in DNSs, and u_{rms} is the root-mean-square velocity. In this state, the Reynolds number $Re = u_{rms}/(k_f \nu)$; most studies quote the value of Re rather than $\mathcal{G}$.

It is convenient to use periodic boundary conditions, if we are not considering the effects of bounding walls, for instance, in studies of statistically homogeneous and isotropic turbulence. For the case with walls we refer the reader to Ref. 54. For a periodic domain, it is best to solve the 2D NS equation by using the pseudospectral method,[53,184] with the 2/3 rule for dealiasing; the successful implementation of such a pseudospectral method relies on efficient, fast-Fourier-transform (FFT) schemes.[185] High-order, finite-difference schemes, like the pencil code[186] can also be used to study turbulence here. Time marching can be carried out by using a variety of schemes including the Adams-Bashforth, fourth-order Runge-Kutta, or exponential Runge-Kutta methods.[187]

From $\omega(\mathbf{x}, t)$, we calculate the total fluid kinetic energy $E(t)$ and the fluid-energy dissipation rate $\varepsilon(t)$ as follows:

$$E(t) = \langle |\mathbf{u}(\mathbf{x}, t)|^2 \rangle_{\mathbf{x}}, \qquad (2)$$

$$\varepsilon(t) = \langle \nu |\omega(\mathbf{x}, t)|^2 \rangle_{\mathbf{x}}, \qquad (3)$$

where the average over space is shown by $\langle \rangle_{\mathbf{x}}$. We then obtain (a) the root-mean-square fluid velocity, $u_{rms} = \sqrt{\langle 2E(t) \rangle_t}$, where $\langle \rangle_t$ indicates the time average over the turbulent, but statistically steady state of the fluid, (b) the Taylor-microscale Reynolds number $Re_\lambda(t) = \sqrt{2}E(t)/\sqrt{\nu \varepsilon(t)}$, and the mean $\langle Re_\lambda \rangle_t$, and (c) the box-size eddy-turnover time $\tau_{eddy} = L/u_{rms}$. It is often convenient to scale time by τ_{eddy}. The energy spectrum of the fluid is

$$E(k) \equiv \sum_{k-\frac{1}{2} \leq k' \leq k+\frac{1}{2}} \langle |\hat{\mathbf{u}}(\mathbf{k}', t)|^2 \rangle_t, \qquad (4)$$

where the circumflex denotes the spatial Fourier transform. We also calculate the Okubo-Weiss parameter[54,188,189]

$$\Lambda = (\omega^2 - \sigma^2)/8, \qquad (5)$$

where $\sigma^2 = \sum_{i,j} \sigma_{ij}\sigma_{ji}$, with $\sigma_{ij} = (\partial_i u_j + \partial_j u_i)$, where i and j indicate Cartesian components; in the inviscid, unforced case without friction, the flow is vortical, if $\Lambda > 0$, or extensional (strain-dominated), if $\Lambda < 0$. The Okubo-Weiss criterion works well even in the presence of viscosity, friction, and forcing.[54]

The multiscaling properties of turbulence are often characterized by the equal-time, order-p, longitudinal-velocity structure function

$$\mathcal{S}_p(r) \equiv \langle [\delta u_{\parallel}(r, t)]^p \rangle, \qquad (6)$$

where $\delta u_{\parallel}(r, t) \equiv [\mathbf{u}(\mathbf{x}+\mathbf{r}, t) - \mathbf{u}(\mathbf{x}, t) \cdot \mathbf{r}/r]$ and $r \equiv |\mathbf{r}|$. In the inertial range (e.g., $\eta_d \ll r \ll L$ for the case of 3D turbulence, with η_d the Kolmogorov dissipation scale), $\mathcal{S}_p(r) \sim r^{\zeta_p}$, where ζ_p is the equal-time exponent. Vorticity structure functions can be defined similarly; they play an important role in characterizing multiscaling in the forward-cascade regime in 2D fluid turbulence (see the subsection on dynamic multiscaling in Sec. III).

To study the dynamics of a small, rigid, circular disk or *inertial* particle in an incompressible flow,[73,74] we use the following equations,[75] if the particle is much heavier than the advecting fluid:

$$\frac{d}{dt}\mathbf{x}(t) = \mathbf{v}(t), \qquad (7)$$

$$\frac{d}{dt}\mathbf{v}(t) = -\frac{\mathbf{v}(t) - \mathbf{u}(\mathbf{x}, t)}{\tau_s}, \qquad (8)$$

$\mathbf{v}$ and $\mathbf{x}$ are, respectively, the velocity and position of an inertial particle, $\tau_s = (2R_p^2 \rho_p)/(9\nu \rho_f)$ is the Stokes (or response) time of the particle of radius R_p, density ρ_p in a fluid of density ρ_f. The Stokes number $St = \tau_s/\tau_\eta$, where τ_η is the Kolmogorov dissipation time. We also assume the following: $R_p \ll \eta$, where η is the Kolmogorov dissipation scale of the carrier fluid; there are no interactions between particles because the particle-number density is low; the acceleration because of gravity can be neglected relative to the turbulence-induced acceleration of the particles. For a neutrally buoyant tracer or Lagrangian particle, $\mathbf{v}(t) = \mathbf{u}(\mathbf{x}, t)$, so

$$\frac{d}{dt}\mathbf{x}(t) = \mathbf{u}(\mathbf{x}, t). \qquad (9)$$

The statistical properties of the tracers are interesting in themselves; in addition, they help us to define quasi-Lagrangian fields that are required to study dynamic multiscaling (see below).

To go beyond circular disks, we can consider neutrally buoyant elliptical particles,[101] whose center of mass satisfies

$$\frac{d}{dt}\mathbf{x}_c = \mathbf{u}(\mathbf{x}_c(t), t), \qquad (10)$$

and the time evolution of the orientation follows the Jeffery equation,[101] which is, in 2D,

$$\frac{d}{dt}\Theta = \frac{1}{2}\omega + \upsilon(\varrho)[\sin(2\Theta)S_{11} - \cos(2\Theta)S_{12}], \qquad (11)$$

where Θ gives the orientation of the semimajor axis relative to a fixed direction, $S_{ij} = \sigma_{ij}/2$, the components of the rate-of-strain tensor are evaluated at $\mathbf{x}_c$, $\upsilon(\varrho) \equiv (\varrho^2 - 1)/(\varrho^2 + 1)$, ϱ is the ratio of the lengths of the semi-major and semi-minor axes of the ellipse, and (circular disks) $0 \leq \upsilon \leq 1$ (thin needles).

For the statistical properties of the particle paths, we follow the trajectories of N_p particles in DNSs. Trilinear interpolation can be used to calculate the velocity and the velocity-gradient tensor at the particle positions. We obtain the trajectories of these particles via an Euler scheme, which suffices, if, in one time step, a particle crosses only a small fraction of the grid spacing.

B. Magnetohydrodynamics

The statistical properties of 2D MHD turbulence have been studied for several decades.[103–117] They employ the equations of incompressible 2D magnetohydrodynamics (MHD) that are [cf. Eq. (1) for the 2D NS case]

$$\frac{\partial \omega}{\partial t} + \mathbf{u} \cdot \nabla \omega + \alpha^\omega \omega = -\nu(-\nabla^2)^\varsigma \omega + f^\omega + \mathbf{b} \cdot \nabla j,$$

$$\frac{\partial \psi^b}{\partial t} + \mathbf{u} \cdot \nabla \psi^b + \alpha^{\psi^b} \psi^b = -\eta^b(-\nabla^2)^\varsigma \psi^b + f^{\psi^b}, \qquad (12)$$

where **b**, the magnetic field, and **u**, the velocity field, follow from the 2D analog of the magnetic vector potential ψ^b and the stream function ψ: $\mathbf{b} = \hat{z} \times \nabla \psi^b$ and $\mathbf{u} = \hat{z} \times \nabla \psi$, where $\hat{z}$ is the unit vector perpendicular to the 2D domain; $j = \nabla^2 \psi^b$ and $\omega = \nabla^2 \psi$ are, respectively, the current density and vorticity. These equations satisfy the incompressibility condition $\nabla \cdot \mathbf{u} = 0$ and $\nabla \cdot \mathbf{b} = 0$. We allow for dissipativity of order ς, friction with coefficients α^ω and α^{ψ^b}; and ν and η^b are, respectively, the kinematic viscosity and magnetic diffusivity; f^ω and f^{ψ^b} are the forcing terms. {We follow Ref. 115 with some changes in notations to ensure consistency across this paper; for example, Ref. 115 uses ψ for the 2D analog of the magnetic vector potential, but we use ψ^b [cf. their Eq. (5)].}

In addition to Re, the nondimensionalized friction, and k_f, we have other control parameters here. They are the magnetic Prandtl number $Pr_M = \nu/\eta^b$ and the friction-coefficient ratio $\alpha^\omega/\alpha^{\psi^b}$. If we use hyperviscosity and hyperdiffusivity, i.e., $\varsigma > 1$, it is useful to define the effective viscosity and magnetic diffusivity,[115] respectively,

$$\nu_{\text{eff}} = \frac{\sum_k \nu k^{2\varsigma} E^u(k)}{\sum_k k^2 E^u(k)},$$

$$\eta^b_{\text{eff}} = \frac{\sum_k \eta^b k^{2\varsigma} E^b(k)}{\sum_k k^2 E^b(k)}, \quad (13)$$

here the fluid- and magnetic-energy spectra $E^u(k)$ and $E^b(k)$, respectively, are defined like their fluid counterparts.[115] The effective magnetic Prandtl number is $Pr_{M;\text{eff}} = \nu_{\text{eff}}/\eta^b_{\text{eff}}$. To the best of our knowledge, there is no comprehensive study of 2D MHD turbulence that explores a large range of values of Pr_M and friction coefficients.

The results we present in the MHD subsection of Sec. III are based, principally, on the two pseudospectral DNSs of Ref. 115, which use the conventional pseudospectral method[105,184] in a doubly periodic, square simulation domain and a 2/3 dealiasing method, and time marching via a second-order, Runge-Kutta method. The first of these DNSs uses $\varsigma = 2$, to obtain large inertial ranges in energy spectra; furthermore, $\alpha^\omega = 0$ but $\alpha^{\psi^b} > 0$ to suppress the accumulation of magnetic energy at small k in the magnetic-energy spectrum $E^b(k)$. The second DNS uses the conventional values $\varsigma = 1$, $\alpha^\omega = \alpha^{\psi^b} = 0$, so the inverse cascade in ψ^b leads to a small-k accumulation of magnetic energy. For other parameters see Table I in Ref. 115. We emphasize that long runs are required to obtain statistically steady states, whose statistical properties are characterized by the fluid and magnetic energies, their energy spectra $E^u(k)$ and $E^b(k)$, respectively, PDFs of the Okubo-Weiss parameter, and its magnetic analog, which can be defined like their fluid counterparts.[115]

C. Fluid with polymer additives

Dilute polymer solutions are modeled by using viscoelastic models in which the polymer contribution to the fluid is represented by an extra stress term in the NS equations.[125,126,133,136–142,190–192] This stress is expressed in terms of the polymer-conformation tensor $\mathcal{C}$, which is advected by the velocity field of the fluid. Some studies employ the linear, Oldroyd-B model for polymers because of its simplicity, but this model has a limitation because it allows polymers

to stretch without bound. The finitely extensible-nonlinear-elastic-Peterlin (FENE-P) model overcomes this limitation by approximating a polymer by a nonlinear dumbbell, which has a single relaxation time τ_P and a maximal extension L_P. For a recent discussion of the FENE-P model, albeit in the 3D case, we refer the reader to Ref. 192, which discusses its derivation and the limitations of this model.

We concentrate on the 2D, coupled, incompressible NS and FENE-P equations, which we write in terms of the streamfunction ψ and the vorticity $\omega = \nabla \times \mathbf{u}(\mathbf{x}, t)$ as follows:

$$D_t \omega = \nu \nabla^2 \omega + \frac{\mu_P}{\tau_P} \nabla \times \nabla \cdot [f(r_P)\mathcal{C}] - \alpha\omega + F^\omega, \quad (14)$$

$$\nabla^2 \psi = \omega, \quad (15)$$

$$D_t \mathcal{C} = \mathcal{C} \cdot (\nabla \mathbf{u}) + (\nabla \mathbf{u})^T \cdot \mathcal{C} - \frac{f(r_P)\mathcal{C} - \mathcal{I}}{\tau_P}. \quad (16)$$

Here, $D_t \equiv \partial_t + \mathbf{u} \cdot \nabla$, and, as in the incompressible 2D NS equation, the uniform solvent density $\rho = 1$, α and ν are, respectively, the friction coefficient and the kinematic viscosity; μ_P is the zero-shear viscosity parameter for the solute (FENE-P); F^ω is the forcing term. We often use the Kolmogorov-type form $F^\omega = k_f F^0 \cos(k_f y)$, with amplitude F^0, as in the experiments of Ref. 135, for which the energy-injection wave vector is k_f; the superscript T denotes a transpose, $\mathcal{C}_{\beta\beta'} \equiv \langle R_\beta R_{\beta'} \rangle$ are the elements of the polymer-conformation tensor (angular brackets indicate an average over polymer configurations), $\mathcal{I}$ is the identity tensor, $f(r_P) \equiv (L_P^2 - 2)/(L_P^2 - r_P^2)$ is the FENE-P potential, and $r_P \equiv \sqrt{\text{Tr}(\mathcal{C})}$ is the length of the polymers.[140,141] If we set $f(r_P) = 1$, we get the Oldroyd-B model.[142]

In addition to the parameters Re and $k_f/k_{\max}$, which we use in classical-fluid turbulence, we have other important non-dimensional parameters here. They are $c \equiv \mu_P/(\nu + \mu_P)$, a dimensionless measure of the polymer concentration,[191] the scaled polymer extension r_P/L_P, and the Weissenberg number Wi, the ratio of the polymer time scale τ_P to a typical shearing time scale in the turbulent fluid; for example, we can set Wi $= \tau_P \sqrt{\epsilon^f/\nu}$, with ϵ^f the energy dissipation rate for the fluid; other choices can lead to slightly different values for Wi; for example, τ_P can be multiplied by the maximum Lyapunov exponent of the flow to obtain a Weissenberg number based on this Lyapunov exponent.[192] To characterize dissipation reduction (see below), it is useful to calculate the energy $\mathcal{E}(t) \equiv \langle \frac{1}{2}|\mathbf{u}(\mathbf{x},t)|^2 \rangle_{\mathbf{x}}$, the enstrophy $\Omega(t) \equiv \langle \frac{1}{2}|\omega(\mathbf{x},t)|^2 \rangle_{\mathbf{x}}$, and the mean-square palinstrophy $\mathcal{P}(t) \equiv \langle \frac{1}{2}|\nabla \times \omega(\mathbf{x},t)|^2 \rangle_{\mathbf{x}}$, where $\langle \rangle_{\mathbf{x}}$ denotes a spatial average, the PDFs of scaled polymer extensions $P(r_P/L)$, ω^2, σ^2, and the Okubo-Weiss parameter Λ.

In our DNSs of 2D fluid turbulence with polymer additives,[140,141] we use periodic boundary conditions on a square simulation domain and the following numerical scheme to solve the FENE-P equations: for time marching, the fourth-order, Runge-Kutta scheme; in space an explicit, fourth-order, central-finite-difference scheme. Furthermore, we use the Kurganov-Tadmor (KT) shock-capturing scheme for the advection term in Eq. (16) [see Eq. (7) of Ref. 126] to resolve steep gradients in the components of $\mathcal{C}$ and, thereby, minimize dispersion errors, whose size increases with L_P and τ_P. Equation (15) is solved conveniently by a Fourier-space method. It is important to pick a sufficiently small time step[140]

to maintain $r_P \leq L_P$. It is equally important to ensure that the symmetric-positive-definite (SPD) nature of $\mathcal{C}$ is preserved by the numerical scheme. This is best done[140,141] by using a 2D variant of the Cholesky-decomposition scheme of Refs. 125, 126, and 191; this scheme exploits the property that any SPD matrix can be written as the product of a lower-triangular matrix and its transpose; Eqs. (14)–(16) can then be recast in terms of the components of a lower-triangular matrix; the SPD nature of the parent matrix is, therefore, manifestly maintained at every stage of the DNS (see Ref. 140 for the 2D case). A straightforward pseudospectral DNS does not maintain this SPD property of $\mathcal{C}$ at every step.

D. Binary-fluid mixture

The Cahn-Hilliard (CH)[147] equation is of fundamental importance in the statistical mechanics of binary mixtures, where it has been used to study phase transitions, critical phenomena, nucleation, spinodal decomposition, and phase separation or coarsening.[143–154] For a binary mixture, whose two components are fluids, the CH and NS are coupled to obtain the Cahn-Hilliard- Navier-Stokes (CHNS) equations (also called model H[145]). These equations allow us to follow the spatiotemporal evolution of the two fluids and the interfaces between them; we do not have to impose boundary conditions on these moving interfaces because they are diffuse; but, in the CHNS system, we have, in addition to the NS velocity field, a scalar, order-parameter field ϕ, which is negative in one phase and positive in the other; interfacial regions between these phases exhibit large gradients in ϕ.

Coupling, between a minority-phase droplet and the majority-phase (background) fluid, appears naturally in the CHNS equations.[155,193–197] In the terminology of the particles-in-turbulent-flows literature,[78] this is a four-way coupling: the droplets are advected by the background fluid, which they affect in turn; furthermore, droplets can interact or fuse with each other, or a single droplet can break into small fragments. Note that most studies of particles in turbulent flows consider particles whose linear size is well below the Kolmogorov dissipation scale of the flow; the droplets we consider in our CHNS studies have sizes that lie in the inertial range of scales, where energy spectra show power-law forms.

In 2D, the CHNS equations can be written in the following vorticity formulation:[155,156]

$$(\partial_t + \mathbf{u} \cdot \nabla) \omega = \nu \nabla^2 \omega - \alpha \omega - \nabla \times (\phi \nabla \mu) + F^\omega, \quad (17)$$

$$(\partial_t + \mathbf{u} \cdot \nabla) \phi = \gamma \nabla^2 \mu \text{ and } \nabla \cdot \mathbf{u} = 0. \quad (18)$$

Here, $\mathbf{u} \equiv (u_x, u_y)$, the fluid velocity; ω, the vorticity, and μ, the chemical potential are given by[155,193]

$$\omega = (\nabla \times \mathbf{u})\hat{\mathbf{e}}_z, \quad (19)$$

$$\mu(\mathbf{x}, t) = \delta \mathcal{F}[\phi]/\delta\phi, \quad (20)$$

$$\mathcal{F}[\phi] = \Lambda \int [(\phi^2 - 1)^2/(4\xi^2) + |\nabla\phi|^2/2]d\mathbf{x}, \quad (21)$$

where $\mathcal{F}[\phi]$ is the Cahn-Hilliard free energy, the two phases mix in the interfacial regime with energy density Λ, the diffuse interface width $\sim \xi$, ν is the kinematic viscosity, γ is the mobility[195] of the mixture, the Kolmogorov-type forcing $F^\omega = F^0 \cos(k_f y)$ has amplitude F^0 and forcing wave number

k_f, and α is the air-drag induced friction. For simplicity, we take γ to be independent of ϕ and both components to have the same viscosity. The surface tension $\sigma = \frac{2\sqrt{2}\Lambda}{3\xi}$ and the Grashof number $Gr = \frac{L^4 F^0}{\nu^2}$ is the dimensionless ratio of the forcing and viscous terms; the diffusivity $D = \frac{\gamma\Lambda}{\xi^2}$ (we do not vary this here). If a gravity term is added to the right-hand side of the CHNS equation, it can be used to study Rayleigh-Taylor turbulence[193] in 2D, if the density difference between the two fluids is small.

The 2D CHNS model has many more control parameters than those we have discussed for the 2D NS case. These are as follows: (a) The forcing-scale $l_f = 2\pi/k_f$ Weber number $We \equiv \rho l_f^3 F^0/\sigma$, a natural dimensionless measure of the inverse of the surface tension; (b) the non-dimensionalized interface width or Cahn number $Ch = \xi/L$; (c) the mean value of ϕ (e.g., if this is zero, we have a symmetric or 50-50 mixture; if it is significantly different from zero, we can have a droplet of the minority phase in a background of the majority phase); (d) the capillary number $Ca = \frac{3\varepsilon\nu\rho u_{rms}}{2\sqrt{2}\sigma}$, the ratio between the viscous and capillary forces; (e) the Peclet number $Pe = (L\varepsilon^2 u_{rms})/(\sigma\gamma)$, the ratio of the diffusive and the convective time-scales; and (f) if we include gravity,[193] then we also have the Atwood number, the ratio between the difference and the sum of the densities of the two fluids.

If we study the spatiotemporal evolution of a droplet in the CHNS system, it is convenient to begin with the following order-parameter profile:[155,193,194]

$$\phi(x, y) = \tanh\left[\frac{1}{\sqrt{2}\xi}\left(\sqrt{(x - x_c)^2 + (y - y_c)^2} - d_0/2\right)\right]; \quad (22)$$

this yields, at $t = 0$, a circular droplet, with its center at (x_c, y_c) and diameter d_0; it has a diffuse interface, with width ξ, which is best expressed by the Cahn number $Ch = \xi/L$. The scaled, initial droplet diameter d_0/L is yet another control parameter for DNSs that are designed to investigate droplet dynamics. Detailed studies of the dependence of the statistical properties of 2D CHNS turbulence on all these control parameters remain a challenge; such comprehensive studies are now being attempted.[155–157,198]

Our DNSs of the CHNS equations follow Refs. 155, 156, and 198. In particular, we use the pseudospectral method and periodic boundary conditions in a square simulation domain; because of the cubic nonlinearity, we use $N/2$-dealiasing;[184] and for time marching, we use the exponential Adams-Bashforth method ETD2.[187] We have developed both MPI codes, for parallel computers, and a CUDA[199] code for use on computers with graphics processing units (e.g., the NVIDIA K80); these efficient codes allow us to explore the large parameter space for the 2D CHNS system and carry out very long simulations. Parameters for our studies are given in Refs. 155, 156, and 198.

In the following paragraph, we introduce the quantities that we calculate from the fields $\omega(\mathbf{x},t)$ and $\phi(\mathbf{x},t)$, which we obtain from our DNSs of the CHNS equations.

From $\phi(\mathbf{x}, t)$, we obtain the droplet-deformation parameter[155,200]

$$\Gamma(t) = \frac{\mathcal{S}(t)}{\mathcal{S}_0(t)} - 1, \quad (23)$$

where $\mathcal{S}(t)$ is the perimeter of the droplet (the $\phi = 0$ contour) at time t, $\mathcal{S}_0(t)$ is the perimeter of an undeformed droplet of equal area at t. From the field $\omega(\mathbf{x}, t)$, we calculate, for the fluid, $E(t)$, $\varepsilon(t)$, u_{rms}, $Re_\lambda(t)$, $\langle Re_\lambda \rangle_t$, $E(k)$, and τ_{eddy} as in the 2D NS case; we express time in units of τ_{eddy}. Now it is also useful to obtain the order-parameter (or phase-field) spectrum:

$$S(k) \equiv \sum_{k-\frac{1}{2} \le k' \le k+\frac{1}{2}} \langle |\hat{\phi}(\mathbf{k}', t)|^2 \rangle_t, \qquad (24)$$

where the circumflex denotes spatial Fourier transforms.

E. Two-fluid HVBK model

The theoretical model that we use for the dynamics of a superfluid depends on the length scales we consider. For length scales much larger than both the core of a quantum vortex and the mean separation between such vortices, the incompressible Hall-Vinen-Bekharevich-Khalatnikov (HVBK), two-fluid model[162–168,201] can be used, if we consider low-Mach-number situations. Strictly speaking, we can only have power-law, Kosterlitz-Thouless superfluid ordering at finite temperatures in 2D;[143,144] this subtlety comes out clearly in the Gross-Pitaevskii (GP) description that we present in Subsection II F. However, on the time scales of experiments on finite samples, an HVBK description may well suffice, if we consider the length scales mentioned above. It is in this sense that it is useful to study 2D superfluid turbulence via the 2D HVBK model.

In essence, the HVBK model consist of the incompressible Navier-Stokes equation (for the normal fluid) coupled with an Euler equation (for the superfluid) via a *mutual-friction* term. The incompressible, 2D HVBK equations are[162–166]

$$D_t \mathbf{u}_n = -\frac{1}{\rho_n}\nabla p_n + \nu_n \nabla^2 \mathbf{u}_n - \mu_n \mathbf{u}_n + \mathbf{F}_{mf}^n + \mathbf{f}_u^n, \quad (25a)$$

$$D_t \mathbf{u}_s = -\frac{1}{\rho_s}\nabla p_s + \nu_s \nabla^2 \mathbf{u}_s - \mu_s \mathbf{u}_s + \mathbf{F}_{mf}^s + \mathbf{f}_u^s. \quad (25b)$$

Here, $D_t \mathbf{u}_i \equiv \partial_t + \mathbf{u}_i \cdot \nabla$, incompressibility imposes $\nabla \cdot \mathbf{u}_i = 0$, the subscript $i \in (n, s)$ distinguishes normal-fluid (n) and superfluid (s) components, which have the density, partial pressure, and viscosity ρ_i, p_i, and ν_i, respectively; the coefficients μ_i account for friction. For the superfluid, ν_s and μ_s are, of course, zero; however, in any DNS, we must use $\nu_s(\neq 0) \ll \nu_n$ and $\mu_s \ll \mu_n$ to avoid numerical instabilities in the statistically steady state of superfluid turbulence. $\mathbf{F}_{mf}^n = (\rho_s/\rho)\mathbf{f}_{mf}$ and $\mathbf{F}_{mf}^s = -(\rho_n/\rho)\mathbf{f}_{mf}$ are the mutual-friction terms, where

$$\mathbf{f}_{mf} = \frac{B}{2}\frac{\omega_s}{|\omega_s|} \times (\omega_s \times \mathbf{u}_{ns}) + \frac{B'}{2}\omega_s \times \mathbf{u}_{ns}, \qquad (26)$$

with the slip velocity $\mathbf{u}_{ns} = (\mathbf{u}_n - \mathbf{u}_s)$; the mutual-friction coefficients are B and B'. These have been measured, as functions of temperature, in 3D experiments,[201] but such measurements have not been made in 2D. Therefore, we often set $B' = 0$ (so, in 2D, $\mathbf{f}_{mf} = -\frac{B}{2}|\omega_s|\mathbf{u}_{ns}$) but check in a representative case that, if $B' > 0$, our qualitative conclusions do not change.

In our DNS of the 2D HVBK system, we use the stream-function ψ_i and vorticity $\omega_i = \nabla \times \mathbf{u}_i = -\nabla^2 \psi_i$ formulation,[54] force the vorticity fields with Kolmogorov-type terms $f_\omega^i = -f_0^i k_f^i \cos(k_f^i x)$ and f_0^i and k_f^i amplitudes and the forcing wave

number, respectively. We use (a) $k_f^i = 2$ and (b) $k_f^i = 50$ to study energy spectra that are dominated, respectively, by a forward- or an inverse-cascade regime; in case (b), we force the normal-fluid (superfluid) component if $\rho_n/\rho > 0.5$ ($\rho_n/\rho \le 0.5$). We use periodic boundary conditions, on a square simulation domain, the pseudospectral method[54,168] with the 2/3 dealiasing rule, and, for time marching, a second-order, exponential time differencing Runge-Kutta method.[187] The parameters of our DNSs are given in Ref. 168, which we follow closely here.

We characterize the statistical properties of homogeneous isotropic turbulence in the 2D HVBK model by computing the energy spectra $E_n(k)$ and $E_s(k)$, $E_i(k) = \langle \sum_{k-\frac{1}{2} < k' \le k+\frac{1}{2}} |\mathbf{u}_i(\mathbf{k}', t)|^2 \rangle_t$ ($\langle \rangle_t$ denotes the time average), various probability distribution functions (PDFs) like $P(\omega_i)$, for the vorticities, and the PDF of the cosine of the angle θ between $\mathbf{u}_n$ and $\mathbf{u}_s$, and energy and enstrophy fluxes and the mutual-friction transfer function $M_i(k)$, for which we refer the reader to Ref. 168.

F. Gross-Pitaevskii superfluid

To resolve spatial scales of the order of the core size of a quantum vortex, we can use the Gross-Pitaevskii (GP) equation for the spatiotemporal evolution of a weakly interacting Bose superfluid, at low temperatures. The GP equation is well known (see, e.g., Refs. 162 and 183 and references therein). We have proposed a minimal Lagrangian[183] that allows us to study the dynamics of active Newtonian particles in a GP Bose superfluid; these particles are active in the sense that they affect the superfluid; their motion is, in turn, affected by the superfluid; furthermore, we allow the particles to have a short-range (SR) repulsion. Our model Lagrangian is

$$\begin{aligned}
\mathcal{L} = \int_{\mathcal{A}} &\Big[\frac{i\hbar}{2}\Big(\Psi^* \frac{\partial \Psi}{\partial t} - \Psi \frac{\partial \Psi^*}{\partial t}\Big) - \frac{\hbar^2}{2m}\nabla \Psi \cdot \nabla \Psi^* \\
&+ \mu|\Psi|^2 - \frac{g}{2}|\Psi|^4 - \sum_{i=1}^{\mathcal{N}_0} V_{\mathcal{P}}(\mathbf{r} - \mathbf{q}_i)|\Psi|^2 \Big] d\mathbf{r} \\
&+ \frac{m_o}{2}\sum_{i=1}^{\mathcal{N}_0} \dot{q}_i^2 - \sum_{i,j,i\neq j}^{\mathcal{N}_0,\mathcal{N}_0} \frac{\Delta_E r_{SR}^{12}}{|\mathbf{q}_i - \mathbf{q}_j|^{12}},
\end{aligned} \qquad (27)$$

where the condensate wave function is Ψ, with Ψ^* its complex conjugate, $\mathcal{A}$ is the simulation domain, g is the effective interaction strength, m is the mass of the bosons, μ is the chemical potential, $V_{\mathcal{P}}$ is the potential that we use to represent the particles, and $\mathcal{N}_0$ is the total number of particles each with mass m_o. The last term in the model Lagrangian above is the SR repulsive, two-particle potential that is characterized by Δ_E and r_{SR}. If we remove the last three terms in this equation, we get the conventional GP equation. The Madelung transformation, $\Psi(\mathbf{r}, t) = \sqrt{\rho(\mathbf{r}, t)/m} \exp(i\Phi(\mathbf{r}, t))$, relates Ψ to the density and phase fields $\rho(\mathbf{r}, t)$ and $\Phi(\mathbf{r}, t)$, respectively, whence we get the superfluid velocity $\mathbf{v}(\mathbf{r}, t) = (\hbar/m)\nabla\Phi(\mathbf{r}, t)$; clearly, such flow is irrotational if there are no vortices.

In the absence of particles, we can now rewrite the total GP energy as

$$E = \int_{\mathcal{A}} \Big[\frac{1}{2}\rho v^2 + \frac{1}{2}g|\Psi|^4 + \frac{\hbar^2}{2m^2}|\nabla\sqrt{\rho}|^2 \Big] d\mathbf{r}, \qquad (28)$$

which has the following parts: the kinetic energy $E_{kin} = (1/2) \int \rho |v|^2 d\mathbf{r}$, the interaction energy $E_{int} = (1/2) \int g|\Psi|^4 d\mathbf{r}$, and the quantum-pressure energy $E_q = (\hbar^2/2m^2) \int |\nabla\sqrt{\rho}|^2 d\mathbf{r}$. We can subdivide the kinetic energy into contributions that come from the compressible (superscript c) and incompressible (superscript i) parts of $\sqrt{\rho}\mathbf{v}$ as follows: We begin with the decomposition $\sqrt{\rho}\mathbf{v} = (\sqrt{\rho}\mathbf{v})^i + (\sqrt{\rho}\mathbf{v})^c$, where $\nabla \cdot (\sqrt{\rho}\mathbf{v})^i = 0$ and $\nabla \times (\sqrt{\rho}\mathbf{v})^c = 0$, whence we get the following compressible and incompressible parts of E_{kin}:

$$E_{kin}^i = \frac{1}{2} \int_{\mathcal{A}} |(\sqrt{\rho}v)^i|^2 d^2x, \tag{29a}$$

$$E_{kin}^c = \frac{1}{2} \int_{\mathcal{A}} |(\sqrt{\rho}v)^c|^2 d^2x. \tag{29b}$$

These energies can be written in terms of their Fourier-space spectra as follows:[174]

$$E_{kin}^i = \frac{1}{2} \int |\widehat{(\rho^{1/2}\mathbf{v})^i}|^2 d^2k \equiv \int E_{kin}^i(k) dk, \tag{30}$$

$$E_{kin}^c = \frac{1}{2} \int |\widehat{(\rho^{1/2}\mathbf{v})^c}|^2 d^2k \equiv \int E_{kin}^c(k) dk, \tag{31}$$

$$E_{int} = \int |\widehat{\sqrt{g/2}|\psi|}|^2 d^2k \equiv \int E_{int}(k) dk, \tag{32}$$

and

$$E_q = \int |\widehat{\nabla\rho^{1/2}}|^2 d^2k \equiv \int E_q(k) dk; \tag{33}$$

here, $\widehat{O}$ denotes the spatial Fourier transform of $O(\mathbf{r})$, k is the wave number, and the time dependence of the spectra has been suppressed. Similarly, we can define the occupation-number spectra via

$$N = \int |\widehat{\Psi}|^2 d^2k \equiv \int n(k) dk. \tag{34}$$

These spectra reach a statistically steady form under the following conditions: (a) if the Fourier-truncated GP equation is used, as in any DNS (see below), and the system thermalizes completely; (b) or the GP equation is forced and then a dissipation mechanism is introduced, at small length scales (large k), in a variety of ways (see, e.g., Refs. 159 and 170–172), to account for different possible dissipation mechanisms that can arise at length scales comparable to or smaller than the healing length. Freely decaying turbulence in the 2D GP equation can also be studied by introducing a dissipation mechanism (e.g., Ref. 202 introduces a hyperviscosity of the type we have discussed above in the MHD context).

Other statistical properties that help us to characterize the statistical properties of the 2D GP system are various PDFs, such as those of the components of the velocity, and the correlation function

$$c(r) = \langle \left[e^{-i\Phi(\mathbf{x})} - \langle e^{-i\Phi(\mathbf{x})} \rangle \right] \left[e^{i\Phi(\mathbf{x+r})} - \langle e^{i\Phi(\mathbf{x+r})} \rangle \right] \rangle, \tag{35}$$

which helps us to identify the Berezinski-Kosterlitz-Thouless (BKT) phase in the thermalized state; in the BKT phase, $c(r)$ decays as a power of $1/r$.

For the particle part of our model Lagrangian above, it is convenient to use the Gaussian potential $V_\mathcal{P} = V_o \exp(-r^2/2d_p^2)$, with strength V_o and width d_p, to represent a particle. The particle displaces some superfluid with mass m_f and, in 2D, an area comparable to the area of the particle. The important control parameter $\mathcal{M} \equiv m_o/m_f$ distinguishes between particles that are (1) heavy ($\mathcal{M} > 1$), (2) neutral ($\mathcal{M} = 1$), and (3) light ($\mathcal{M} < 1$).

To solve the 2D GP equations, we use a pseudospectral DNS,[174,183] a 2D, periodic, square computational domain and a fourth-order, Runge-Kutta scheme for time marching. It is convenient to work with the quantum of circulation $\kappa \equiv h/m \equiv 4\pi\alpha_0$, speed of sound $c_s = \sqrt{2\alpha_0 g\rho_0}$, healing length $\xi = \sqrt{\alpha_0/(g\rho_0)}$, and the mean density ρ_0. Different studies use slightly different normalizations or units. In our calculations with particles,[183] we set $\rho_0 = 1$, $c = 1$, and $\xi = 1.44$ dx, where $dx = L/N_c$, N_c^2 is the number of collocation points, $\mu = g$, $V_o = 10\,g$, $d_p = 1.5\,\xi$, and $\Delta_E = 0.062$.

III. OVERVIEW OF RESULTS

This section is divided into six subsections. The first of these is devoted to some statistical properties of particles that are advected by a turbulent, 2D fluid (Subsection III A). The next one deals with cascades in 2D MHD turbulence (Subsection III B). The third describes the effects of polymer additives in a 2D fluid (Subsection III C). The fourth covers recent studies of 2D binary-fluid turbulence (Subsection III D). The fifth provides an overview of 2D superfluid turbulence at the level of the 2D HVBK equations (Subsection III E). The last one is devoted to results on the statistical properties of turbulence in the 2D GP equation (Subsection III F); we also cover particle dynamics in a 2D GP superfluid.

A. Particles in a 2D turbulent fluid

As we have mentioned above, in 2D fluid turbulence, the inverse and forward cascades[7,53,54,64–66] lead to power-law forms for the energy spectrum that are, respectively,

$$E(k) \sim k^{-5/3}, k_\alpha \ll k \ll k_f, \tag{36}$$

$$E(k) \sim k^{-\delta}, k_f \ll k \ll k_v, \tag{37}$$

here, $k_\alpha \sim \alpha/u_{rms}$ is the small-k (IR) cutoff induced by friction, and $k_v \sim \nu^{-1/2}\eta_\nu^{1/6}$ is the large-k (UV) cutoff, with η_ν the constant enstrophy flux; $\delta = 3$ without friction, but it increases with the friction coefficient because of nonlocal interactions.[7,53,54,64–66] A single DNS can obtain both these power-law ranges[53,55] only if its resolution is very high; an experimental example of both cascades is given in Ref. 41. In the absence of friction, it is not easy to obtain a statistically steady state for forced 2D fluid turbulence. Two, large coherent vortices, with opposite signs if the mean vorticity vanishes, dominate the large-time behavior of the system and its statistical properties evolve slowly in time; however, a very long run[56] has managed to get a statistically steady state in this case.

The parameter-dependence of other statistical properties, especially those in the forward-cascade regime, is discussed in Refs. 7, 53, 54, and 64–66; furthermore, velocity structure functions (see below) do not show significant multi-scaling, but vorticity structure functions do. While calculating such structure functions, it is important to extract their isotropic parts. The PDFs of velocity components are close

to Gaussian; and the PDF for the Okubo-Weiss parameter Λ shows a cusp and its form is in quantitative agreement with experiments.[54]

We turn now to the statistics of passive particles, which are advected by 2D turbulent flows but do not themselves affect the flow. Their dynamics are governed by Eq. (9), for Lagrangian tracers, and Eq. (8), for heavy particles. We can calculate several quantities that characterize (a) the clustering of heavy particles and (b) the geometrical properties, such as the curvature of these trajectories. The clustering of heavy particles, or preferential concentration, in 3D turbulent flows is well known.[72,75,78] This occurs in 2D flows too.[83,84,87,88] Lagrangian tracers are distributed uniformly in the flow. Initially, as the Stokes number St increases, so does the degree of clustering; eventually, at large-enough values of St, the clustering tendency decreases. Formations of network-type regions, with a high density of particles, and empty spaces in between have been reported and analysed in Ref. 88; and it has been suggested that such clustering is correlated with acceleration stagnation points in an inverse-cascade-dominated DNS of 2D fluid turbulence.[87] Studies of single-particle and relative dispersion of particles in 2D turbulent fluids can be found in, e.g., Refs. 79–83. The geometries of particle tracks, in particular the statistics of their curvatures, have been studied in Refs. 85, 86, and 89–91. Irreversibility has also been studied at the single-particle level.[203,204] These studies are well known in the fluid-dynamics literature.

In addition, we can use the trajectories of particles to address questions that are of prime importance in nonequilibrium statistical physics; these issues are not very well known in the fluid-dynamics community, so we concentrate on them here. In particular, we provide a summary of how Lagrangian tracers can be used (a) to define quasi-Lagrangian fields, whose time-dependent structure functions play a central role in establishing the dynamic multiscaling of time-dependent structure functions,[100] and (b) the persistence problem for turbulence.[93]

1. Dynamic multiscaling

It has been noted often that there is a striking similarity between critical phenomena in statistical mechanics[143,144] and the statistical properties of fluid turbulence. For example, in the former, correlation functions show a power-law dependence on the spatial separation between, say, spins in an Ising model, at the critical point. As the system approaches this critical point, its correlation length diverges; the relaxation time too diverges as a power z of the correlation length, leading to *dynamic scaling* with a *dynamic-scaling exponent* z. The fluid-turbulence analog[96–100] of power-law, critical correlation functions is the inertial-range, power-law behavior of the structure functions we have mentioned above.

What time-dependent structure functions should we use to develop the turbulence analog of dynamic scaling? The answer to this important question does not follow immediately by pursuing the standard development of this subject in critical phenomena because of the following two difficulties: (a) We cannot use time-dependent Eulerian structure functions; they lead to trivial dynamic scaling, with an exponent $z = 1$ because of the sweeping effect: roughly speaking, the mean flow of

large eddies sweeps small ones, so spatial and temporal separations are related linearly via the mean-flow velocity. (b) We must characterize the *dynamic multiscaling* of time-dependent structure functions.

To remove sweeping effects, it is natural to use quasi-Lagrangian (superscript ^{QL}) fields.[94–100] These are defined with respect to a Lagrangian particle, which was at the point $\mathbf{R}_0$ at time t_0, and, at time t, is at $\mathbf{R}(t|\mathbf{R}_0, t_0)$, such that $d\mathbf{R}(t|\mathbf{R}_0, t_0)/dt = \mathbf{u}[\mathbf{R}(t|\mathbf{R}_0, t_0), t]$, where $\mathbf{u}$ is the Eulerian velocity. For example, the quasi-Lagrangian velocity field $\mathbf{u}^{QL}$ is

$$\mathbf{u}^{QL}(\mathbf{x}, t|\mathbf{R}_0, t_0) \equiv \mathbf{u}[\mathbf{X} + \mathbf{R}(t|\mathbf{R}_0, t_0), t]; \qquad (38)$$

similarly, we can define its vorticital counterpart ω^{QL} in terms of the Eulerian ω; and, remarkably, we can calculate such quasi-Lagrangian fields in a DNS in both 2D[100] and 3D.[205] We restrict ourselves to 2D here.

We begin with the equal-time, order-p, vorticity structure functions $\mathcal{S}^{\varphi}(r) \equiv \langle [\delta\omega^{\varphi}(r, t)]^p \rangle \sim r^{\zeta^{\varphi}}$, in the power-law range, and with $\delta\omega^{\varphi}(r,t) = [\omega^{\varphi}(\mathbf{x} + \mathbf{r}, t) - \omega^{\varphi}(\mathbf{x}, t)]$; the superscript φ can be E (Eulerian) or QL (quasi-Lagrangian); to avoid cumbersome notation, we suppress the subscript ω on S_p^{φ} and the multiscaling exponent ζ^{φ}. We assume isotropy (Ref. 100 discusses how to extract of the isotropic parts of S_p^{φ} in a DNS). The time-dependent, vorticity structure functions, for order-p, are

$$\mathcal{F}^{\varphi}(r, \{t_1, \ldots, t_p\}) \equiv \langle [\delta\omega^{\varphi}(r, t_1) \cdots \delta\omega^{\varphi}(r, t_p)] \rangle, \qquad (39)$$

in general, $t_1, \ldots, t_p$ are p different times; and $\mathcal{F}^{\varphi}(r, \{t_1 = \cdots = t_p = 0\}) = \mathcal{S}^{\varphi}(r)$. Let us consider the simplest case $t_1 = t$ and $t_2 = \cdots = t_p = 0$ with the time-dependent structure function denoted by $\mathcal{F}^{\varphi}(r, t)$. Given $\mathcal{F}^{\varphi}(r, t)$, we can extract a characteristic time scale $\tau_p(r)$ from its integrals or derivatives (see below); and we can use these time scales to define and obtain the dynamic-multiscaling exponents z_p via the *dynamic-multiscaling Ansatz* $\tau_p(r) \sim r^{z_p}$. We obtain order-p, degree-M, *integral* (superscript I) or *derivative* (superscript D) time scales by using Eqs. (40) and (41) below,

$$\mathcal{T}_{p,M}^{I,\varphi}(r) \equiv \left[\frac{1}{\mathcal{S}^{\varphi}(r)} \int_0^{\infty} \mathcal{F}^{\varphi}(r, t) t^{(M-1)} dt \right]^{(1/M)}, \qquad (40)$$

$$\mathcal{T}_{p,M}^{D,\varphi} \equiv \left[\frac{1}{\mathcal{S}^{\varphi}(r)} \frac{\partial^M}{\partial t^M} \mathcal{F}^{\varphi}(r, t) \Big|_{t=0} \right]^{(-1/M)}, \qquad (41)$$

and thence we calculate the dynamic-multiscaling exponents $z_{p,M}^{I,\varphi}$, via $\mathcal{T}_{p,M}^{I,\varphi} \sim r^{z_{p,M}^{I,\varphi}}$, and $z_{p,M}^{D,\varphi}$, via $\mathcal{T}_{p,M}^{D,\varphi} \sim r^{z_{p,M}^{D,\varphi}}$.

Equal-time vorticity structure functions in 2D fluid turbulence with friction exhibit multiscaling in the direct cascade range.[54,64,65] A generalization of the multifractal model,[5] with time-dependent velocity structure functions in 3D,[95,96,98,99] yields linear *bridge relations* between dynamic-multiscaling and equal-time exponents. For our 2D direct-cascade regime, with friction, these bridge relations for vorticity-structure-function exponents are[100]

$$z_{p,M}^{I,\varphi} = 1 + [\zeta_{p-M}^{\varphi} - \zeta^{\varphi}]/M, \qquad (42)$$

$$z_{p,M}^{D,\varphi} = 1 + [\zeta^{\varphi} - \zeta_{p+M}^{\varphi}]/M. \qquad (43)$$

The DNS of Ref. 100, to which we refer the reader for details, allows us to compute both equal-time and dynamic-multiscaling exponents and to verify that the bridge relations
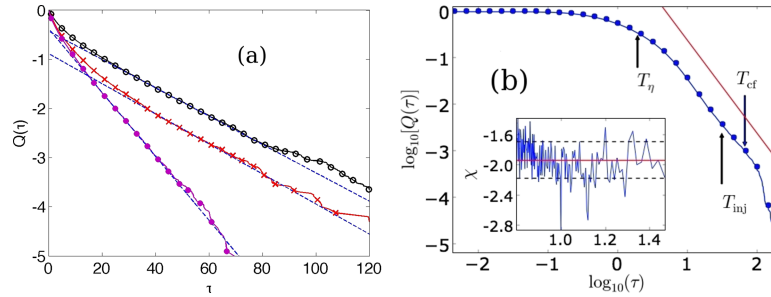
FIG. 1. (a) Illustrative semilog plots of the persistence-time cumulative PDFs Q_E^+ (red crosses), Q_E^- (black open circles), and Q_L^- (magenta full circles); here E and L denote Eulerian and Lagrangian frames, respectively; and + or − PDFs from vortical ($\Lambda > 0$) and extensional ($\Lambda < 0$) regions, respectively; dashed lines are exponential fits. (b) A representative log-log plot of the cumulative PDF $Q_L^+(\bullet)$ versus τ showing the power-law region whose slope yields the persistence exponent [see Fig. 2 of Ref. 93 for details and definitions of T_η, $T_{\rm inj}$, and $T_{\rm cf}$ and the local-slope analysis (inset) of the power-law regime]. Reproduced with permission from Perlekar *et al.*, "The persistence problem in two-dimensional fluid turbulence," Phys. Rev. Lett. **106**, 054501 (2011). Copyright 2011 American Physical Society.

of Eqs. (42) and (43) above are satisfied, within error bars (see Table I in Ref. 100).

2. The persistence problem

Another problem that has attracted a lot of interest in nonequilibrium statistical mechanics is the persistence problem.[92] To define this, we consider a field Υ and obtain the persistence-time PDF $P^\Upsilon(\tau)$, which is the probability that the sign of Υ, at a point, does not change up until a time τ. Studies show that for a variety of systems, $P^\Upsilon(\tau) \sim \tau^{-\vartheta}$ as $\tau \to \infty$ where ϑ is called the *persistence exponent*; it has been obtained analytically only for a few models;[92] for most models, this exponent has to be calculated numerically. A natural way of defining and calculating the persistence exponent in 2D turbulence has been given in Ref. 93, which uses the Okubo-Weiss parameter Λ to distinguish between vortical ($\Lambda > 0$) and extensional ($\Lambda < 0$) regions in the 2D flow. Persistence times are then defined in the following frameworks: (A) Eulerian framework: consider the time evolution of Λ, at a point (x, y), and determine the time τ for which the flow at (x, y) remains vortical (extensional) if, at this point, it became vortical (extensional) at some earlier time; (B) Lagrangian framework: obtain the time τ for which a Lagrangian particle resides in a vortical (extensional) region if it entered that region at an earlier time.

The DNS study of Ref. 93 obtains PDFs and cumulative PDFs, denoted generically by Q, of τ. In the Eulerian framework, these PDFs show exponential tails, both with $\Lambda > 0$ and $\Lambda < 0$ [see, e.g., Fig. 1(a)]. In the Lagrangian framework, the PDF of the residence time of the particle in extensional regions also shows an exponential tail. In contrast, the analogous PDF for vortical regions shows *a power-law region* that is clearly apparent in Fig. 1(b). This power law, which stems from the long time for which a passive particle can be trapped in a vortical region,[93] yields the persistence exponent $\vartheta = 2.9 \pm 0.2$; this exponent appears to be universal, insofar as it is independent of Re, k_f, and α. The detailed verification and elucidation of such universality remains an important challenge. Furthermore, characteristic lifetimes can be obtained from the persistence-time PDFs that decay exponentially.[93] (A 3D generalization has been discussed recently;[206] here all persistence-time PDFs fall exponentially.) We refer the reader

to Ref. 90, which also studies Lagrangian-tracer statistics conditioned on the topology of the flow, characterized, as in our work, via the sign of Λ.

3. Elliptical particles

The last example we give of the rich statistical properties of particles in 2D turbulent flows considers elliptical tracers as in Ref. 101; this DNS study employs forcing either (A) at large or (B) intermediate length scales; cases (A) and (B) lead to qualitatively different properties. With forcing (A), particle orientations form large-scale structures in space; these are absent for forcing (B). The unit vector, along the semi-major axis of an elliptical particle, **p** and $\nabla \times \omega$ align more with forcing (A) than with forcing (B), as we show by the illustrative plots of the PDFs of χ, the angle between **p** and $\nabla \times \omega$, in Fig. 2. Furthermore, this alignment is much weaker than its 3D analog, i.e., the alignment of **p**, for ellipsoidal particles, and ω, which is yet another difference between turbulence in 2D and 3D. Reference 101 calculates many other statistical properties of orientation and rotation dynamics of these elliptical tracers. We highlight one of these, which uses the order-parameter correlation function from the statistical physics of liquid crystals in 2D, namely, $\Gamma(r) = [\langle \mathcal{P}(\mathbf{r}, t)\mathcal{P}(\mathbf{0}, t)\rangle - \langle \mathcal{P}(\mathbf{r}, t)\rangle\langle \mathcal{P}(\mathbf{0}, t)\rangle]/\langle \mathcal{P}^2\rangle$,
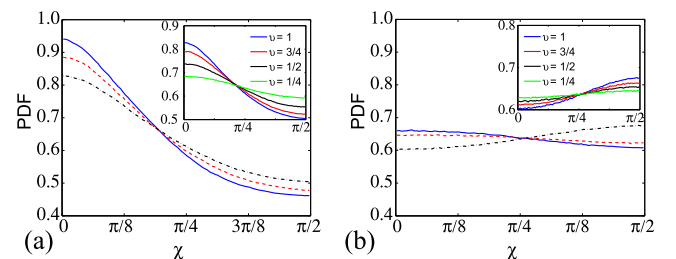

FIG. 2. PDFs of the angle χ between $\boldsymbol{p}$ and $\boldsymbol{\nabla} \times \boldsymbol{\omega}$. Left: run A1 (solid, blue curve), run A2 (dashed, red curve), run A3 (dotted-dashed, black curve) for $\upsilon = 1$. The inset shows the same PDF for run A3 and different values of υ. Right: run B1 (solid, blue curve), run B2 (dashed, red curve), run B3 (dotted-dashed, black curve) for $\upsilon = 1$. The inset shows the same PDF for run B3 and different values of υ. For run numbers and details, see Ref. 101, which uses the symbol γ instead of υ. Reproduced with permission from A. Gupta, D. Vincenzi, and R. Pandit, "Elliptical tracers in two-dimensional, homogeneous, isotropic statistics of alignment, rotation, and nematic order," Phys. Rev. E **89**, 021001(R) (2014). Copyright 2014 American Physical Society.
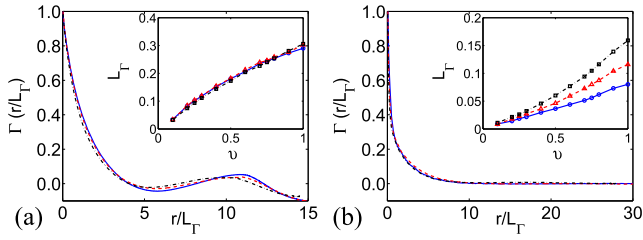
FIG. 3. Single-time two-point correlation function of $\mathcal{P}$ as a function of the space separation rescaled by the correlation length. Left: run A1 (solid, blue curve), run A2 (dashed, red curve), run A3 (dotted-dashed, black curve) for $\upsilon = 1$. Right: run B1 (solid, blue curve), run B2 (dashed, red curve), run B3 (dotted-dashed, black curve) for $\upsilon = 1$. The insets show the correlation length as a function of υ; the color code is the same as in the main plots. For run numbers and details, see Ref. 101, which uses the symbol γ instead of υ. Reproduced with permission from A. Gupta, D. Vincenzi, and R. Pandit, "Elliptical tracers in two-dimensional, homogeneous, isotropic statistics of alignment, rotation, and nematic order," Phys. Rev. E **89**, 021001(R) (2014). Copyright 2014 American Physical Society.

where $\mathcal{P}(\mathbf{r}, t) \equiv (2\cos^2\Theta(\mathbf{r}, t) - 1)$ is the local nematic order parameter in 2D.[143] The plots of $\Gamma(r)$ in Fig. 3 show that it oscillates for forcing (A) but decays exponentially for forcing (B). From Γ we can calculate the correlation length L_Γ, which increases with υ, and which goes from 0 (for circular disks) to 1 (for thin needles). Furthermore, in case (A), L_Γ is determined principally by k_f; in case (B), the size of large-scale flow structures increases with Re_λ, so L_Γ increases too.

B. Two-dimensional MHD turbulence

Inverse and forward cascades occur in homogeneous, isotropic, and statistically steady magnetohydrodynamic (MHD) turbulence, in both 3D[102] and 2D. We discuss the statistical properties of 2D MHD turbulence, in which there is an inverse cascade of the magnetic vector potential; this has attracted considerable attention.[103–117] For discussions of the early studies of 2D MHD turbulence, we refer the reader to Refs. 63 and 110, which cover the literature until 2003-2004. The quadratic invariants of ideal, unforced 2D MHD are the total energy, cross helicity, and the mean square vector potential. In 2D MHD, with forcing and a viscosity and magnetic diffusivity, there is a forward cascade of energy and cross helicity, but an inverse cascade in the spectrum for

the vector potential. There have been different suggestions for the scaling forms of the spectra. We concentrate on the inverse-cascade regime and show that the power-law exponents, for the inverse-cascade regime, can depend on dissipation parameters.

The dimensional predictions for the spectra $|\psi^b|^2(k)$, $E^u(k)$, and $E^b(k)$ in this inverse-cascade regime in 2D MHD are[105,111,112,115]

$$|\psi^b(k)|^2 \sim k^{-7/3}, \tag{44}$$

$$E^b(k) \sim k^2|\psi^b(k)|^2 \sim k^{-1/3}, \tag{45}$$

$$E^u(k) \sim E^b(k) \sim k^{-1/3}. \tag{46}$$

The last scaling form for $E^u(k)$ relies on more assumptions than the normal ones that enter such dimensional arguments. For example, it has been suggested[111,112] that the nonlinear terms in the velocity equation in 2D MHD balance each other, to yield the last of the relations in Eq. (46). Another study has suggested[105] that this last argument may not be valid in the inverse-cascade regime, but only in the forward-cascade part, via an Alfvén-type effect from the large-scale magnetic field, which couples small-scale velocity and magnetic fields strongly, so $E^u(k) \sim E^b(k)$. [Roughly speaking, we can relate $E^u(k)$ and $E^b(k)$, in the forward-cascade regime, by appealing to the Alfvén effect, which arises from the influence of the magnetic field, from the largest length scales in the direct numerical simulation, on the fields at small length scales. In particular, the velocity and magnetic fields are tightly coupled, to form Alfvén waves, so $E^u(k) \simeq E^b(k)$. However, such an Alfvén effect should be weak in the inverse-cascade regime because the large-scale magnetic field is not present here.[105]]

The DNS study of 2D MHD in Ref. 115 has been designed to explore, *inter alia*, the inverse-cascade, power-law forms of such spectra; two cases are investigated: R1, with a finite, positive friction, hyperviscosity, and magnetic hyperdiffusivity and R2, with zero friction. This study finds, remarkably, that these runs yield qualitatively different statistical properties; for example, run R1 yields an inverse-cascade regime consistent with $E^u(k) \sim k^0$ and $E^b(k) \sim k^{-1/3}$ (left panel of Fig. 4); however, R2 yields spectra that are consistent with $E^u(k) \sim k^{1/3}$ and $E^b(k) \sim k^{-1/3}$ (right panel of Fig. 4). To get reliable statistically steady states, it is necessary to
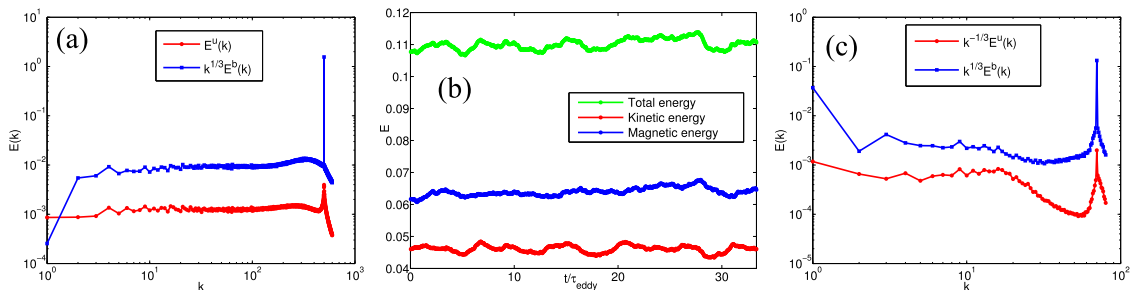

FIG. 4. Log-log plots versus the wave number k, for runs R1 (left panel $k_f = 500$) and R2 (right panel $k_f = 70$); red and blue curves show, respectively, kinetic-energy $E^u(k)$ and magnetic-energy $E^b(k)$ spectra. Middle panel: Plots versus scaled time t/τ_{eddy}, for run R2, of the total energy (green curve), magnetic-energy (blue curve), and kinetic-energy (red curve). For details of these runs see Ref. 115. Reproduced with permission from D. Banerjee and R. Pandit, "Statistics of the inverse-cascade regime in two-dimensional magnetohydrodynamic turbulence," Phys. Rev. E **90**, 013018 (2014). Copyright 2014 American Physical Society.

have very long runs, especially in run R2 (central panel of Fig. 4).

The comparison of results from different DNSs is often not straightforward. We illustrate this by contrasting our results for spectra with those of Refs. 105, 111, and 112. Our spectral exponents from R2 agree with those of Ref. 105, but there are important differences at small k, which suggests that they use a friction unlike our run R2 (we have not found this stated explicitly in their paper). Furthermore, Ref. 105 does employ hyperviscosity ($\varsigma = 2$), whereas our run R2 uses conventional viscosity. Although hyperviscosity can yield a large inertial range, it can also lead to bottlenecks,[207] so we expect that the spectra of Ref. 105 should differ from those of our run R2 only at large values of k, beyond the bottleneck region. The spectral exponents of Refs. 111 and 112 agree with those from our run R2 for $E^u(k)$ but not for $E^b(k)$. Their low-k spectra suggest that they use a friction term or large-scale dissipation. They also report a forward-cascade power-law $E^u(k) \sim k^{-5/3}$; we use a large value of k_f to enhance the size of the inverse-cascade range, so we cannot reliably comment on the forward-cascade regime. The dependence of such exponents on friction and the type of dissipation is known already for the forward-cascade regime in 2D fluid turbulence, where the spectral exponent depends on the friction (see above). Furthermore, in the recent studies of Refs. 116 and 117, the direction of the cascade has been changed by tuning the ratio of the forcing terms in velocity and magnetic-field equations in 2D MHD. Clearly, more high-resolution DNS studies are required to understand all the subtleties of spectra in 2D MHD. Most DNSs of 2D MHD set the magnetic Prandtl number to unity; it is interesting, but challenging, to move away from this value (for the case of 3D MHD see, e.g., Ref. 208).

The study of Ref. 115 also obtains various PDFs that characterize statistically steady 2D MHD turbulence. We present a few illustrative PDFs in Fig. 5. The left panel shows the PDF of $\cos(\beta_{u,b})$, where $\beta_{u,b}$ is the angle between the velocity and the magnetic field; this clearly indicates a tendency for these two vectors to be aligned and, therefore, a depletion of nonlinearities as discussed, e.g., in Ref. 210. The middle and right panels of Fig. 5 show, for runs R1 and R2, PDFs of the Okubo-Weiss parameter Λ and its analog Λ_b for 2D MHD; these plots are qualitatively similar to their 2D-fluid counterparts; and, just as the sign of Λ distinguishes between

vortical and extensional regions in a flow, the sign of Λ_b can be used to test if a region is current-dominated or dominated by magnetic strain.

C. Two-dimensional fluid turbulence with polymer additives

In 3D, fluid flows with small concentrations of polymer additives have been studied extensively because of remarkable, polymer-induced effects, such as drag reduction,[118] in turbulent flows, and elastic turbulence,[119,120] which occurs at low Reynolds numbers. In statistically homogeneous and isotropic turbulence, polymers reduce the dissipation, change the fluid energy spectrum, and suppress small-scale structures.[122–132]

These effects have also been studied in 2D flows via experiments[133–135] and DNSs.[136–141] It is now possible to carry out (a) high-resolution[140] DNSs of the FENE-P model (Subsection II C) or (b) long DNSs for substantial ranges[141] in the Weissenberg (Wi) number and Reynolds (Re) number parameter space. We give illustrative results from these studies to show how well we can capture the effects of polymers on a turbulent 2D fluid and uncover the crossover from dissipation-reduction to elastic-turbulence regimes in the Wi-Re parameter space.

Figure 6(a) shows dissipation-reduction-type phenomena,[140] on the addition of polymers, for they reduce the total fluid energy $\mathcal{E}$ (top panel), the enstrophy Ω (middle panel), and the mean-square palinstrophy $\mathcal{P}$ (bottom panel). The polymers change the fluid energy spectrum in Fig. 6(b) in both inverse- and forward-cascade parts: it is reduced slightly at small and intermediate wave numbers k and enhanced *significantly* at large k (as in its 3D counterpart[125,126]); such spectral features can be identified unambiguously only in a high-resolution DNS like the one in Ref. 140 with $16\,384^2$ collocation points.

The size of a polymer, even when stretched, is less than the dissipation scale. Roughly speaking, the polymers stretch by taking energy from the fluid energy; this then cascades from small to large k; thus, $E(k)$ is depleted at small k. As the polymers relax, they give energy to the fluid at large k and enhance, thereby, the large-k tail of $E(k)$. These qualitative arguments can be quantified by calculating[125,126,130,140] the effective, scale-dependent viscosity $\nu_e(k) \equiv \nu + \Delta\nu(k)$, with
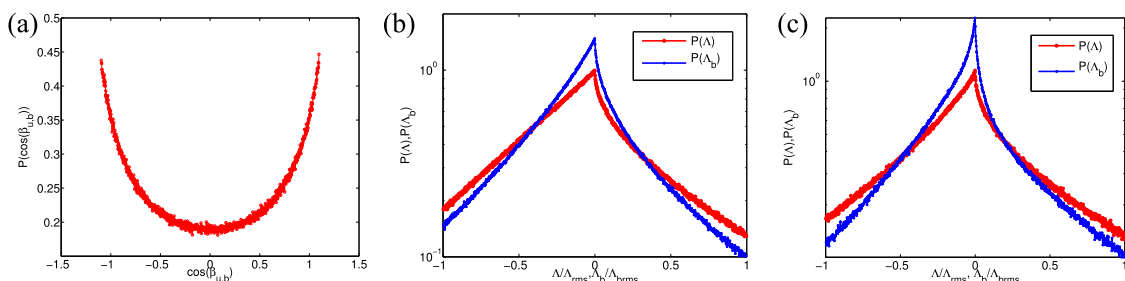

FIG. 5. Plots of the PDFs: Left panel: PDF of $\cos(\beta_{u,b})$, with $\beta_{u,b}$ the angle between **u** and **b**. Middle and right panels: PDFs of Λ (red) and Λ_b (blue) for runs R1 and R2, respectively. For details of these runs see Ref. 115. Reproduced with permission from D. Banerjee and R. Pandit, "Statistics of the inverse-cascade regime in two-dimensional magnetohydrodynamic turbulence," Phys. Rev. E **90**, 013018 (2014). Copyright 2014 American Physical Society.
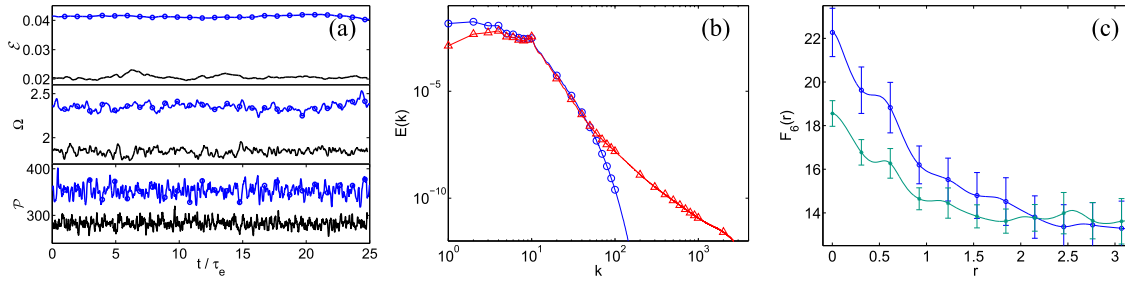
FIG. 6. (a) Plots versus the scaled time t/τ_e of the total kinetic energy $\mathcal{E}$ of the fluid (top panel), the enstrophy Ω (middle panel), and the mean-square palinstrophy $\mathcal{P}$ (bottom panel) for $c = 0$ (upper curve, blue circles for run R7) and $c = 0.4$ (lower curve, black line for run R7); (b) log-log (base 10) plots of the energy spectra $E(k)$ versus k for $c = 0.2$ (red triangles for run R10) and $c = 0$ (blue circles for run R10); (c) plots of the hyperflatness $F_6(r)$ versus r for $c = 0$ (blue circles for run R7) and $c = 0.2$ (green asterisks for run R7) (here run numbers are as in Ref. 140). Reproduced with permission from A. Gupta, P. Perlekar, and R. Pandit, "Two-dimensional homogeneous isotropic fluid turbulence with polymer additives," Phys. Rev. E **91**, 033013 (2015). Copyright 2015 American Physical Society.

$$\Delta\nu(k) \equiv -\mu \sum_{k-1/2 < k' \leq k+1/2} \frac{\mathbf{u}_{\mathbf{k}'} \cdot (\nabla \cdot \mathcal{J})_{-\mathbf{k}'}}{[\tau_P k^2 E^p(k)]}, \quad (47)$$

where the subscripts $\mathbf{k}'$ denote spatial Fourier transforms and $\mathcal{J} = f(r_P)\mathcal{C}$. It can then be shown[140] that $\Delta\nu(k) > 0$, for small k, where $E^p(k) < E^f(k)$, but $\Delta\nu(k) < 0$, at large k, where $E^p(k) > E^f(k)$; the superscripts on E denote the fluid without (f) and with (p) polymers.

Intermittency at small length scales is characterized in the DNS of Ref. 140 by a plot of the hyperflatness $F_6(r)$ [Fig. 6(c)], which shows a marked reduction at small length scales because of polymer additives. Furthermore, the stretching of the polymer by the turbulent fluid can be studied by the conditional PDF of (r_P/L_P), conditioned on the sign of the Okubo-Weiss parameter Λ, which illustrates [Fig. 7(a)] that polymers stretch preferentially in strain-dominated ($\Lambda < 0$) regions. This can also be shown visually by a superimposition of contours of r_P^2 on a pseudocolor plot of Λ [Fig. 7(b)]. Finally, the PDFs of Λ, with and without polymers, show how the tails of these PDFs are depleted on the addition of polymers [Fig. 7(c)].

We turn now to explorations of the disordering of a periodic arrangement of vortices and antivortices in a fluid film by fluid turbulence or by elastic turbulence. We follow Refs. 141 and 211, which characterize this as turbulence- or elastic-turbulence-induced melting of a vortex crystal; such a melting transition is a nonequilibrium analog of the equilibrium, temperature-induced melting of a crystal into a liquid. To study

this problem, we use a DNS of the FENE-P model, with a forcing term such that, without polymers and at low Re, the steady state is a cellular flow, i.e., a square lattice of periodically arranged vortices and anti-vortices. As we increase the Weissenberg number Wi, we find a sequence of nonequilibrium phase transitions, which transforms the original vortex lattice: first we get spatially distorted, but temporally steady, crystals; then a sequence of crystals that oscillate in time, periodically, at low Wi, and quasiperiodically, for slightly larger Wi (these are examples of spatiotemporal crystals, which have no analog in equilibrium statistical mechanics). Finally, the system becomes disordered and displays spatiotemporal chaos and elastic turbulence. There might well be many nonequilibrium states in this system, but only a limited number can be examined in any set of DNSs. We follow Ref. 141 and define the following. SX: original, steady square crystal (the pattern depends on the spatial periodicity of the forcing term); SXA: temporally steady crystals distorted slightly compared to SX; OPXA: crystal, distorted slightly relative to SX, and with periodic temporal oscillations; OQPXA: like OPXA but with quasiperiodic temporal oscillations; SCT: disordered phase with spatiotemporal chaos and turbulence. These states can be characterized in several ways, including nonequilibrium generalizations of order parameters that are used in the density-wave theory of the equilibrium freezing transition from a liquid to a crystal.[141,201,211] We restrict ourselves to plots of (a) the time evolution of the energy $E(t)$, (b) its power spectrum $|E(f)|$ versus the frequency f, and (c) pseudocolor plots of the
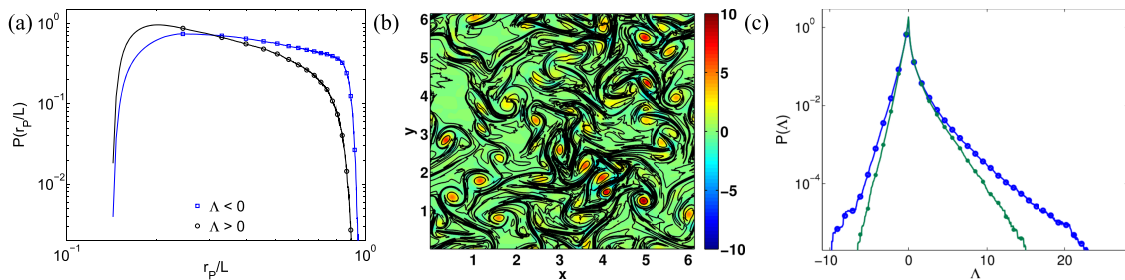

FIG. 7. (a) Conditional PDF of (r_P/L) conditioned on the sign of Λ for run R9; (b) a pseudocolor plot of Λ superimposed on a contour plot of r_P^2 for run R10; (c) PDFs of Λ without (blue curve) and with (green curve) polymers for run R7. For parameters for these runs see Ref. 140. Reproduced with permission from A. Gupta, P. Perlekar, and R. Pandit, "Two-dimensional homogeneous isotropic fluid turbulence with polymer additives," Phys. Rev. E **91**, 033013 (2015). Copyright 2015 American Physical Society.
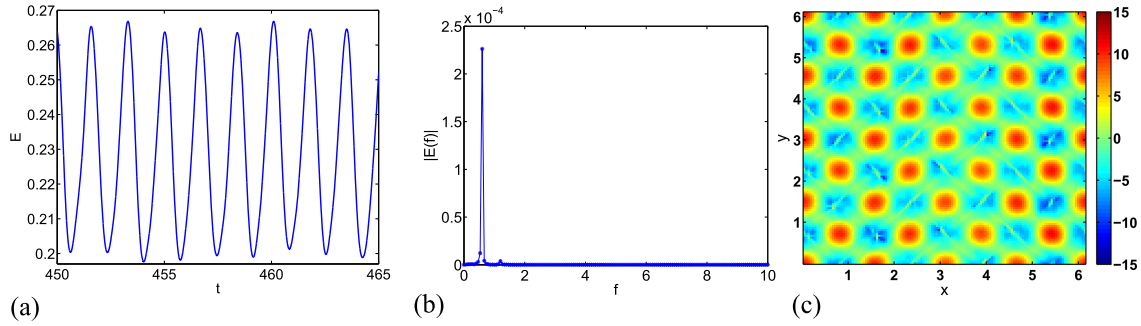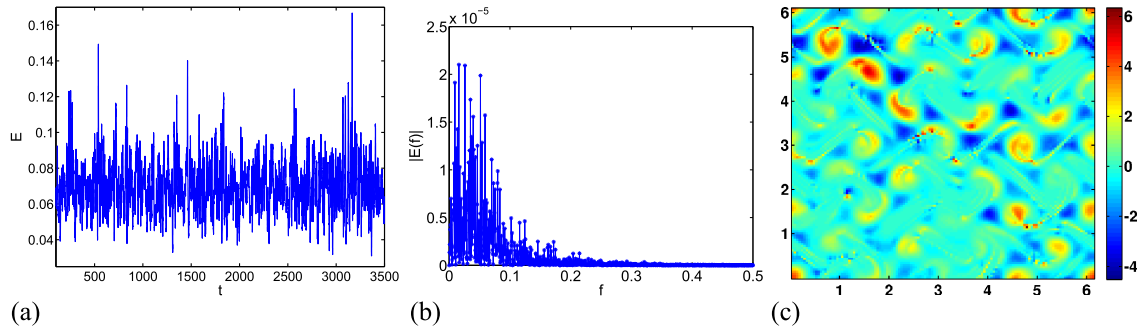
FIG. 8. Plots for an OPXA state ($\Omega = 1$ and Wi = 3): (a) the time evolution of the energy $E(t)$, (b) its power spectrum $|E(f)|$ versus the frequency f, and (c) pseudocolor plots of the Okubo-Weiss parameter Λ; see Ref. 141 for parameters and details. Reproduced with permission from A. Gupta and R. Pandit, "Melting of a nonequilibrium vortex crystal in a fluid film with polymers: Elastic versus fluid turbulence," Phys. Rev. E **95**, 033119 (2017). Copyright 2017 American Physical Society.

FIG. 9. Plots for an SCT state ($\Omega = 1$ and Wi = 20): (a) the time evolution of the energy $E(t)$, (b) its power spectrum $|E(f)|$ versus the frequency f, and (c) pseudocolor plots of the Okubo-Weiss parameter Λ; see Ref. 141 for parameters and details. Reproduced with permission from A. Gupta and R. Pandit, "Melting of a nonequilibrium vortex crystal in a fluid film with polymers: Elastic versus fluid turbulence," Phys. Rev. E **95**, 033119 (2017). Copyright 2017 American Physical Society.

Okubo-Weiss parameter Λ; illustrative plots for OPXA and SCT states are given, respectively, in Figs. 8 and 9.

To examine the stability of these states, 400 DNSs have been carried out in Ref. 141 to obtain the nonequilibrium phase diagram in the Wi-Ω plane [Fig. 10(a)], where $\Omega \propto$ Re. It is important to note that (a) the boundary between the crystalline and turbulent phases has a complicated, fractal-type character and (b) the Okubo-Weiss parameter Λ provides us with a natural measure for characterizing the phases and transitions in this diagram. Such a crystal can be melted in many ways: (A) by increasing Re at low Wi (turbulence-induced melting), as

shown in the absence of polymers in Refs. 85, 86, and 210; the disordered phase is a turbulent fluid that shows dissipation reduction because of the polymer additives; (B) by increasing Wi, at low Re (elastic-turbulence-induced melting); the disordered state is a polymeric fluid that shows elastic turbulence[119] or rheochaos;[120] (C) by increasing both Wi and Re, the disordered state is a polymeric fluid that lies in the crossover regime between dissipation-reduction and elastic-turbulence regimes. The DNS of Ref. 141 characterizes these regimes by using many measures. Illustrative examples include energy spectra [Fig. 10(b)], in different regimes, and plots of contours of r_P^2
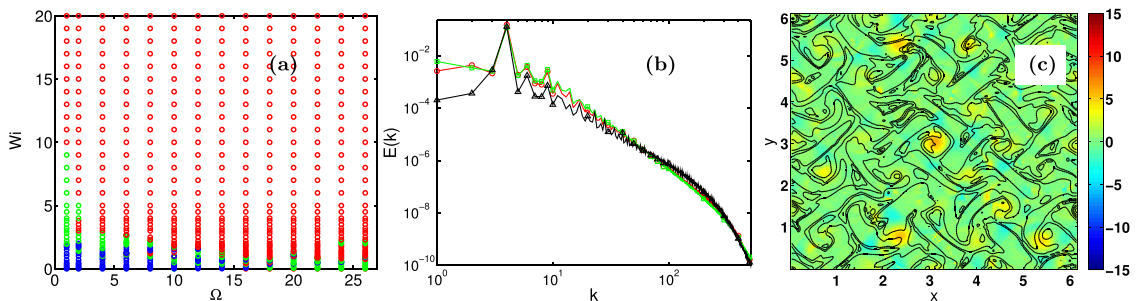

FIG. 10. (a) Phase diagram of our 2D system with polymer additives in the Wi-Ω plane, where blue circles represent the regions SX and SXA, green circles represent the regions OPXA and OQPXA, and the red circles represent the region SCT, (b) plots of energy spectra $E(k)$ versus k and for $\Omega = 4$ and Wi = 10 (red line with circles), $\Omega = 4$ and Wi = 40 (green line with squares), and $\Omega = 50$ and Wi = 5 (black line with triangles) and (c) plots of contours of the polymer stretching r_P^2 superimposed on a pseudocolor plot of the Okubo-Weiss field Λ for $\Omega = 1$ and Wi = 20 (melted crystal in the elastic-turbulence regime); see Ref. 141 for parameters and details. Reproduced with permission from A. Gupta and R. Pandit, "Melting of a nonequilibrium vortex crystal in a fluid film with polymers: Elastic versus fluid turbulence," Phys. Rev. E **95**, 033119 (2017). Copyright 2017 American Physical Society.
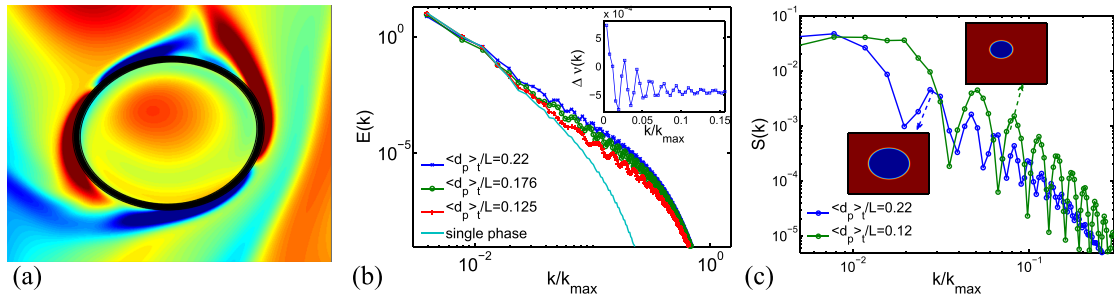
FIG. 11. (a) Pseudocolor plots of the vorticity field with ϕ-field contours superimposed on them; log-log plots (base 10) versus the scaled wavenumber $k/k_{\max}$ of (b) $E(k)$ for runs R12 ($\langle d_p \rangle_t/L = 0.22$, deep-blue line with asterisks), R16 ($\langle d_p \rangle_t/L = 0.176$, green line with crosses), R20 ($\langle d_p \rangle_t/L = 0.125$, red line with circles), and R1 (single-phase fluid, light blue line); the power-laws $k^{-3.6}$ and $k^{-5.2}$ are depicted by yellow-dashdot and black-dashed lines, respectively; (c) the order-parameter spectrum $S(k) = |\hat\phi(k)|^2$ for $\langle d_p \rangle_t/L = 0.22$ and $\langle d_p \rangle_t/L = 0.12$; see Ref. 155 for parameters and details. Reproduced with permission from Pal *et al.*, "Binary-fluid turbulence: Signatures of multifractal droplet dynamics and dissipation reduction," Phys. Rev. E **93**, 063115 (2016). Copyright 2016 American Physical Society.

superimposed on a pseudocolor plot Λ in the elastic-turbulence regime. As far as we know, elastic-turbulence-induced melting of a vortex crystal has not been explored in experiments, but DNSs have been studying it or related problems;[137,138,141] for example, the Kolmogorov-flow pattern of Refs. 137 and 138 is a one-dimensional crystal in our terminology.

D. Two-dimensional binary-fluid turbulence

We turn now to some representative examples of 2D binary-fluid turbulence that have been studied by using the CHNS system of equations. The mean value of the order-parameter field ϕ is an important parameter in this system. In the first case we consider, this value is such that there is a fluctuating droplet [Fig. 11(a)] of the minority phase in a background majority phase; in the second case, this mean value is such that we have a symmetric, 50-50 mixture, which coarsens and phase separates in the absence of turbulence.

This droplet is clearly not passive; therefore, it modifies the turbulence. The energy spectra $E(k)$, with and without the droplet, shown in Fig. 11(b) illustrate how droplets affect the turbulent fluid.[155] First, $E(k)$ exhibits oscillations, with a period that is related reciprocally to $\simeq \langle d_p \rangle_t$, the mean droplet diameter. Second, the large-k tail of $E(k)$ is enhanced by the droplet, in much the same way as it is by polymer additives;[140] so, not surprisingly, it can be understood by introducing the

scale-dependent effective viscosity $\nu_{eff}(k) = \nu + \Delta\nu(k)$ (in Fourier space), with

$$\Delta\nu(k) \equiv \sum_{k-1/2 < k' \leq k+1/2} \frac{\mathbf{u}_{\mathbf{k}'} \cdot (\phi\nabla\mu)_{-\mathbf{k}'}}{k^2 E(k)} \qquad (48)$$

and $(\phi\nabla\mu)_{\mathbf{k}}$ is the Fourier transform of $(\phi\nabla\mu)$ (see the CHNS equations); the inset of Fig. 11(b) displays $\Delta\nu(k)$ for $\langle d_p \rangle_t/L = 0.324$; for $\Delta\nu(k) > 0$, $E(k)$ is less than its single-phase-fluid value (magenta curve); if $\Delta\nu(k) < 0$, $E(k)$ is greater than its single-phase-fluid value. $\Delta\nu(k)$ changes sign at a value of $k/k_{\max}$ that depends on $\langle d_p \rangle_t/L$; the smaller the value of $\langle d_p \rangle_t/L$, the larger is the value of $k/k_{\max}$ at which $\Delta\nu(k)$ goes from being positive to negative. From our study of 2D fluid turbulence with polymer additives,[140] we can anticipate that the large-k enhancement of $E(k)$ leads to dissipation reduction here, as is shown in Ref. 155. The oscillations in $E(k)$ appear even more clearly in the order-parameter spectrum $S(k)$ [Fig. 11(c)]; for small droplet fluctuations, e.g., when the surface tension is large or $\langle d_p \rangle_t/L$ is small, these oscillations are very well defined.

How does the turbulence affect the droplet? We can answer this question quantitatively in the CHNS system by considering the time evolution of the droplet-deformation parameter $\Gamma(t)$ [Fig. 12(a)], which looks clearly intermittent. Indeed, we find that this time series is multifractal as we can
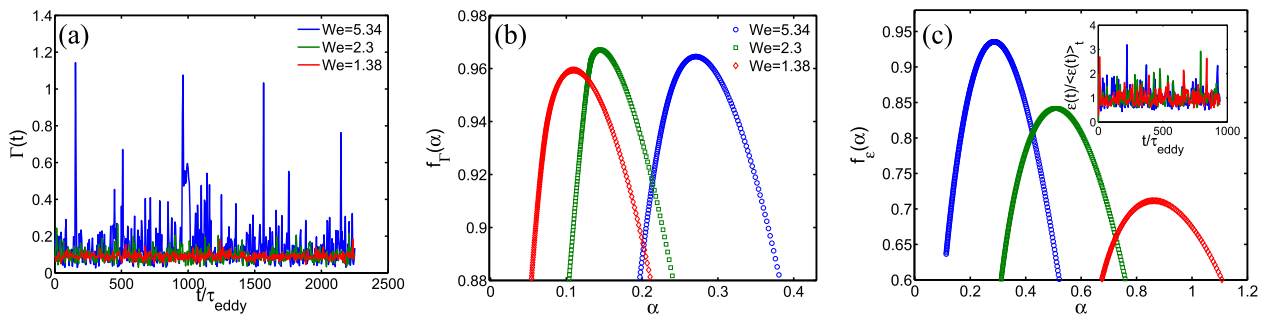

FIG. 12. (a) Plots versus t/τ_{eddy} of $\Gamma(t)$ for the runs R7 ($We = 5.34$, blue line), R8 ($We = 2.3$, green line), and R12 ($We = 1.38$, red line); (b) plots of the multifractal spectra $f_\Gamma(\alpha)$ for the time series of Γ for the runs R7 ($We = 5.34$, blue circles), R8 ($We = 2.3$, green squares), and R13 ($We = 1.38$, red diamonds); (c) plots of the multifractal spectra $f_\varepsilon(\alpha)$ of the energy dissipation $\varepsilon(t)/\langle\varepsilon\rangle_t$ (inset shows the plot versus the scaled time t/τ_{eddy} of the energy dissipation $\varepsilon(t) = \langle\varepsilon\rangle_t$); see Ref. 155 for parameters and details. Reproduced with permission from Pal *et al.*, "Binary-fluid turbulence: Signatures of multifractal droplet dynamics and dissipation reduction," Phys. Rev. E **93**, 063115 (2016). Copyright 2016 American Physical Society.
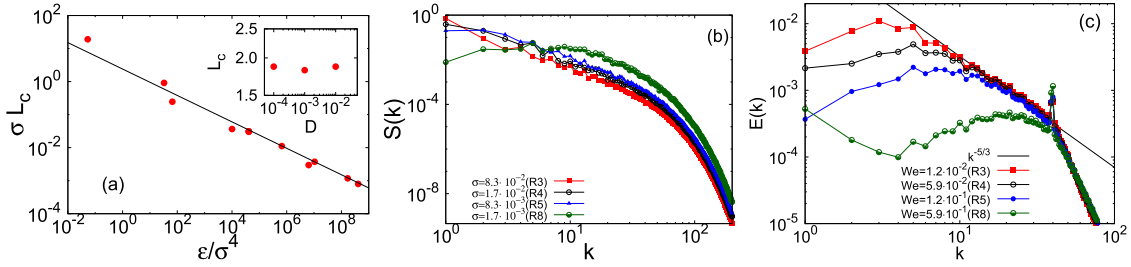
FIG. 13. (a) Log-log (base 10) plots of the spectrum $S(k)$, of the phase-field ϕ, versus k; as σ decreases, the low-k part of $S(k)$ decreases and $S(k)$ develops a broad and gentle maximum whose peak moves out to large values of k. (b) Log-log (base 10) plot of σL_c versus ϵ/σ^4 showing data points [with L_c from $S(k)$] in red; the black line is the Hinze result for L_H (see text); a fit to our data yields an excellent approximation to the arrest scale L_c over several orders of magnitude on both vertical and horizontal axes; the inset shows a plot of L_c versus D. (c) Log-log (base 10) plots of the energy spectrum $E(k)$ versus k, for different values of We, illustrating the truncation of the inverse energy cascade as We increases. The black line indicates the $k^{-5/3}$ result for the inverse-cascade regime in 2D fluid turbulence; see Ref. 156 for parameters and details. Reproduced with permission from P. Perlekar, N. Pal, and R. Pandit, "Two-dimensional turbulence in symmetric binary-fluid mixtures: Coarsening arrest by the inverse cascade," Sci. Rep. **7**, 44589 (2017). Copyright 2017 Nature Publishing Group.

see from the multifractal spectra $f_\Gamma(\alpha)$ [Fig. 12(b)] for the time series of Γ. We have seen already that the droplet modifies the fluid turbulence. Another example of this is given in Fig. 12(c), where we show how the multifractal spectrum $f_\varepsilon(\alpha)$ of the energy dissipation $\varepsilon(t)/\langle \varepsilon \rangle_t$ time series is modified by the droplet.

We now highlight a few results of a CHNS study[156] of the arrest of coarsening in a symmetric (50-50), binary-fluid mixture; we refer the reader to Ref. 156 for details. This work uses parameters that lead, in the absence of the CH-NS coupling, (a) to domain growth or coarsening, which is monitored by ϕ, and (b) an inverse-cascade regime in the energy spectrum $E(k)$. The CH-NS coupling then leads to an arrest of coarsening, at a coarsening-arrest length scale L_c, which is evaluated from the spectrum of ϕ, i.e., $S(k)$ (left panel, Fig. 13), as follows:

$$L_c = 2\pi[\sum_k S(k)]/[\sum_k kS(k)]. \qquad (49)$$

In the middle panel of Fig. 13, we demonstrate that (a) $L_c \sim L_H$, the Hinze scale that follows from balancing inertial and interfacial-tension forces, and (b) L_c is independent, within error bars, of the diffusivity D. (Here, σ denotes the surface or interfacial tension.) We have seen above that ϕ is an active field in the CHNS system, insofar as it acts back on the velocity field. The effect of this back reaction shows up clearly in a modification of the energy spectrum $E(k)$ (right panel, Fig. 13); we see that the inverse energy cascade is now blocked at a wavenumber $k_c \simeq 2\pi/L_c$.

It is also very interesting to note that the symmetric, binary-fluid CHNS system is, in many ways, similar to 2D MHD. We refer the reader to Ref. 156, which contains detailed discussions of the similarities and differences between the 2D MHD and the symmetric CHS system. One of the results of this study is that the mean-square concentration spectrum (2D CHNS) shows the same power law as the mean-square magnetic-potential spectrum, in the inverse-cascade regime of 2D MHD.

E. Two-dimensional HVBK superfluid turbulence

Although the HVBK model has been studied in 3D,[167] a DNS of this model has been carried out in 2D only recently.[168] This offers interesting insights into superfluid turbulence some of which we describe below. The mutual-friction coupling between the normal fluid and the superfluid induces an alignment of these fields. We illustrate this by pseudocolor plots of the vorticity fields (left-side panels of Fig. 14) of ω_n and ω_s from a DNS with $k_f = 2$. This locking of normal-fluid and superfluid fields can be quantified by plotting (right side of Fig. 14) the PDF $P(\cos(\theta))$, with θ the angle between $\mathbf{u}_n(\mathbf{r},t)$ and $\mathbf{u}_s(\mathbf{r}, t)$; clearly, these fields tend to align along the same direction; the degree of alignment increases as we increase the mutual-friction coefficient B. Both normal-fluid and superfluid energy spectra can exhibit inverse- and forward-cascade parts [Figs. 15(a) and 15(b)]. The first of these spectra has $k_f = 2$, so it has a significant forward-cascade part; a comparison of
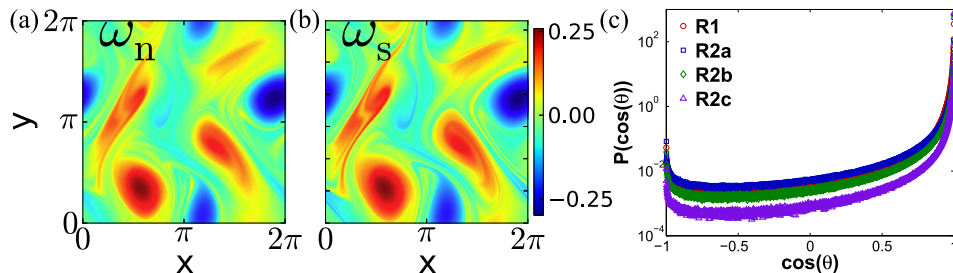

FIG. 14. Pseudocolor plots of the vorticity fields, ω_n and ω_s, from our DNS run R1 at $t = 1720$ [panels (a) and (b), $k_f = 2$]. (c) Semilogarithmic (base 10) plots of the PDF $P(\cos(\theta))$ of the angle θ between $\mathbf{u}_n$ and $\mathbf{u}_s$ for runs R1 (red circles), R2a ($B = 1$, blue squares), R2b ($B = 2$, green diamonds), and R2c ($B = 5$, purple triangles); see Ref. 168 for parameters and details. Reproduced with permission from V. Shukla, A. Gupta, and R. Pandit, "Homogeneous isotropic superfluid turbulence in two dimensions: Inverse and forward cascades in the Hall-Vinen-Bekharevich-Khalatnikov model," Phys. Rev. B **92**, 104510 (2015). Copyright 2015 American Physical Society.
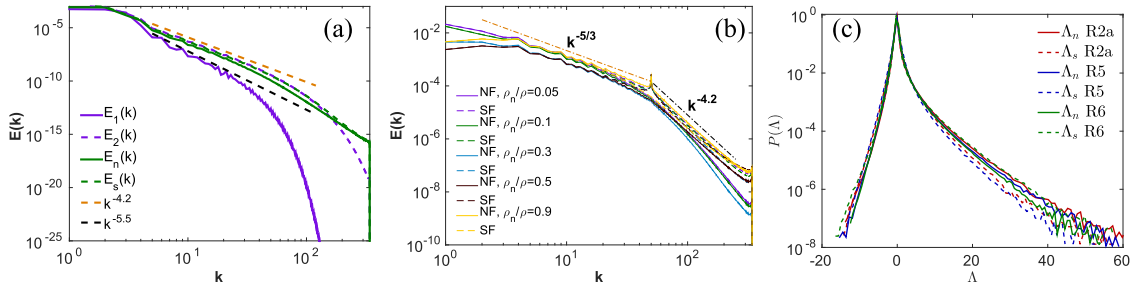
FIG. 15. Log-log plots of the energy spectra $E_n(k)$ (full lines) and $E_s(k)$ (dashed lines) from our DNS runs: (a) R0 ($B = 0$, purple lines) and R1 ($B = 1$, green lines) with $k_f = 2$; (b) R2a (green curves), R3 (purple curves), R4 (sky-blue curves), R5 (brown curves), and R6 (yellow curves), with $B = 1$; we force the dominant component. NF (SF) stands for normal-fluid (superfluid). (c) PDFs of the Okubo-Weiss parameters for runs R2a (red line), R5 (blue line), and R6 (green line), i.e., $\rho_n/\rho = 0.1$, $\rho_n/\rho = 0.5$, and $\rho_n/\rho = 0.9$, respectively; see Ref. 168 for parameters and details. Reproduced with permission from V. Shukla, A. Gupta, and R. Pandit, "Homogeneous isotropic superfluid turbulence in two dimensions: Inverse and forward cascades in the Hall-Vinen-Bekharevich-Khalatnikov model," Phys. Rev. B **92**, 104510 (2015). Copyright 2015 American Physical Society.

$E_n(k)$ (full lines) and $E_s(k)$ (dashed lines), with $B = 0$ (purple lines), with their counterparts for $B = 1$ (green lines) shows again how the two fields and, therefore, their spectra become similar because of the mutual-friction coupling. The spectra in Fig. 15(b) show the dependence of both inverse- and forward-cascade regimes on the normal-fluid fraction ρ_n/ρ. It is also interesting to note that the counterparts here of the Okubo-Weiss parameter have PDFs that are qualitatively similar to their 2D-fluid-turbulence counterparts [Fig. 15(c)]. For details we refer the reader to Ref. 168.

F. Two-dimensional Gross-Pitaevskii superfluid turbulence

There have been several studies of the GP equation in both 3D and 2D (see, e.g., Refs. 159, 160, 162, 174, and 183 and references therein). We give selected results here from recent DNSs of the 2D GP equation (2D GPE), which investigate thermalization in the Fourier-truncated 2D GPE, freely decaying turbulence,[202] and statistically steady turbulence[169–175] in the 2D GPE with some dissipation at small length scales. We end with some results for the 2D GPE with particles.[183]

We first follow the dynamical evolution of the 2D Fourier-truncated GPE, as in Ref. 147, to examine the various stages of its thermalization. For similar studies for the Euler and other hydrodynamical equations, see Refs. 207, 212, and 213; and for the 3D GPE, see Ref. 214. These studies combine ideas from fluid dynamics and statistical mechanics.

In the case of the Fourier-truncated 2D GPE,[174] the time evolution has been classified roughly into four regimes. (A) The first regime is dominated by initial-condition-dependent transients. (B) In the second, power-law regions appear and develop in, e.g., energy spectra; but the exponents and extents of these power-law regions evolve in time and are initial-condition dependent. (C) In regime three, such spectra drop sharply for wave numbers $k > k_c$; partial thermalization occurs for $k < k_c$; the self-truncation wave number $k_c(t)$ grows either as a power of t or as log t (depending on the initial condition). (D) Complete thermalization occurs in regime 4, where a careful consideration of finite-size effects for the correlation function $c(r)$ and spectra show that, at low temperatures, the system shows a Berezinski-Kosterlitz-Thouless phase, as it must in 2D. For a detailed explanation of this process of thermalization, we refer the reader to Ref. 174. Here, we restrict ourselves to two figures that illustrate this process of thermalization for PDFs of the x and y components of the velocity (Fig. 16) and spectra of the compressible kinetic energy $E_c(k)$ (Fig. 17); note the development of the thermalized part of the spectrum that scales as k. The initial condition for the PDFs is such that there are several vortices and anti-vortices initially; these PDFs cross over from a form with power-law tails [Fig. 16(a)] to a Gaussian form [Fig. 16(c)]; such power-law tails in velocity-component PDFs have been seen in experiments and DNSs in 3D; they are associated with the presence of vortices.
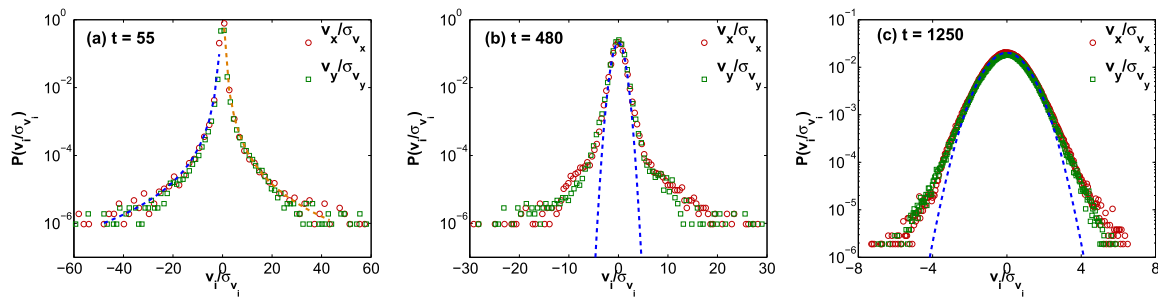

FIG. 16. Semilog (base 10) plots of the PDFs of the x (red circles) and y (green squares) components of the velocity from our DNS runs: (a)–(c) A1 corresponding to the initial conditions IC1. The blue-dashed lines in (b) and (c) indicate fits to Gaussian PDFs; the dashed lines in (a) indicate power-law fits to the left (blue-dashed line) and right (orange-dashed line) tails of the PDFs (see text); see Ref. 174 for parameters and details. Reproduced with permission from V. Shukla, M. Brachet, and R. Pandit, "Turbulence in the two-dimensional Fourier-truncated Gross-Pitaevskii equation," New J. Phys. **15**, 113025 (2013). Copyright 2013 IOP Publishing.

FIG. 17. Log-log (base 10) plots of the spectra $E^c_{kin}(k)$ from our DNS runs (a)–(c) A1 at different times t (indicated by curves of different colours); a k power law, indicating the beginning of thermalization, is shown by orange-dashed lines; see Ref. 174 for parameters and details. Reproduced with permission from V. Shukla, M. Brachet, and R. Pandit, "Turbulence in the two-dimensional Fourier-truncated Gross-Pitaevskii equation," New J. Phys. **15**, 113025 (2013). Copyright 2013 IOP Publishing.
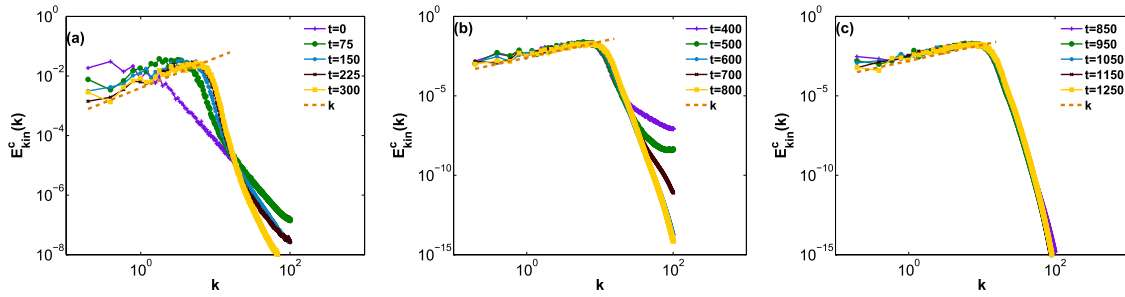
The study of Ref. 202 considers decaying turbulence in the 2D GPE with hyperviscosity (second power of the Laplacian) to investigate if a Bose-Einstein-condensed (BEC) phase occurs beyond an intensity threshold, for the initial condition. This work suggests that, for very weakly nonlinear initial conditions without any visible threshold, BEC arises via a growing phase coherence because of the annihilation of vortices.

The development of an understanding of the nature of the spectral transfer of energy in 2D superfluid turbulence is an important question, which arises, inevitably, when we compare 2D classical-fluid and superfluid turbulence. In particular, does an inverse cascade of energy exist in 2D superfluid turbulence? The search for an answer to this question has led to investigations of vortex dynamics in such systems.[169–175] In a recent experiment on oblate BECs in an annular trap, it has been demonstrated that, on stirring the system at small length scales, of the order of a few healing lengths, the resulting disordered distribution of 2D vortices evolves dissipatively into a large-scale flow.[215] This has been interpreted as a transfer of energy from small to large length scales. Direct numerical simulations of the dissipative Gross-Pitaevskii equation (dGPE), in which a phenomenological dissipation is introduced to model the interaction between the condensate and the thermal bath at finite temperatures, have led to some insights. It has been shown that the existence of an inverse cascade and the

associated scaling exponent is linked to the spatial organization of the vortices, with the same sign of circulation, into clusters, reminiscent of the coherent vortices in 2D, classical-fluid turbulence.[172,176,177] The role played by the vortex distribution and the vortex clusters is still a subject of research.[178–180]

We now discuss one interesting result of a recent study[183] of the collision of two Newtonian particles in a 2D GP superfluid, which evolve according to the model equations (GP with particles) that we have discussed above. This study shows that, in this model, there is an effective, attractive interaction between the particles; this is mediated by the superfluid; it then goes on to investigate, in a DNS, collisions between particles as a function of their incident kinetic energy and the extent of the repulsive force between particles, when they approach close to each other. The study of Ref. 183 finds that there is a transition, as a function of parameters, from almost elastic to completely inelastic collisions; this can be monitored by computing the coefficient of restitution; it also finds that aggregation and clustering result from this sticking transition in multiparticle systems. Figure 18(a) gives a plot of the particle positions $q_{o,x}$ versus the scaled time $c_s t/\xi$, for the case of neutral particles ($\mathcal{M} = 1$). Insets show the sequence of the collision events shown via the pseudocolor plots of the density field $\rho(\mathbf{r})$ (the particles appear as blue disks in which
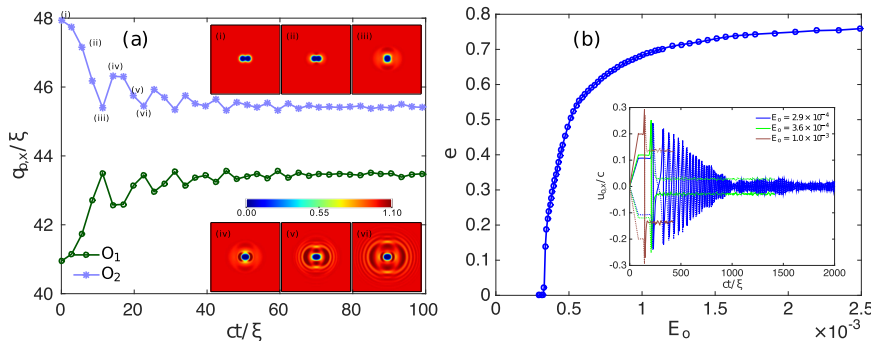

FIG. 18. Superfluid-mediated attractive potential: (a) Plot of the particle ($\mathcal{M} = 1$) positions $q_{o,x}$ versus the scaled time $c_s t/\xi$. Inset: the sequence of the collision events shown via the pseudocolor plots of the density field $\rho(\mathbf{r})$ (the particles appear as blue disks in which $\rho = 0$); particles are released from rest, with an initial separation $r_0 = 7\,\xi$, they undergo multiple collisions with the generation of sound waves in the wake of this collision; and they form a bound state with $r \simeq r_{SR}$; O_1 and O_2 are the particle labels. Energies are in units of $E_\xi = 2\alpha_0\rho_0^2 g$. (b) Plot of the coefficient of restitution e versus E_o for the head-on collision between two heavy particles ($\mathcal{M} = 7.5$). Inset of (b): Plots of the particle velocity $u_{o,x}$ versus t following a head-on collisions between two heavy particles ($\mathcal{M} = 7.5$) for three different values of the incident kinetic energy E_o of each particle, at $r_{SR} = 1.5\,\xi$; see Ref. 183 for parameters and details. Reproduced with permission from V. Shukla, M. Brachet, and R. Pandit, "Sticking transition in a minimal model for the collisions of active particles in quantum fluids," Phys. Rev. A **94**, 041602(R) (2016). Copyright 2016 American Physical Society.

$\rho = 0$). Figure 18(b) displays the coefficient of restitution e versus E_o for the head-on collision between two heavy particles ($\mathcal{M} = 7.5$); the inset here shows the particle velocity $u_{o,x}$ versus t, following head-on collisions, for three different values of the incident kinetic energy E_o of each particle, at $r_{SR} = 1.5\ \xi$. Given this model, it is now possible to study in detail the dynamics of active and interacting particles in the 2D GP superfluid; for the spatio-temporal evolution of multi-particle assemblies interacting with a GP superfluid, we refer the reader to Ref. 183 for details.

IV. CONCLUSIONS

We have presented an overview of the statistical properties of two-dimensional (2D) turbulence in fluids with particles, conducting fluids (2D MHD), fluids with polymer additives (2D FENE-P), binary-fluid mixtures (2D CHNS), and superfluids (2D HVBK or 2D GP), which is based principally on our studies of these problems. It is useful to compare the results of studies of turbulence in these systems to bring out similarities between them, where they exist. Indeed, we have found examples of such similarity, e.g., effective viscosities that lead to drag-reduction-type phenomena in both 2D FENE-P and 2D CHNS systems and the similarities between the 2D CHNS, for the symmetric, 50-50 mixture, and the 2D MHD systems. We have also explored the natures of inverse cascades in some of these systems, e.g., in 2D MHD and 2D HVBK. And we have emphasized how the Okubo-Weiss parameter (and its generalizations) can help us to distinguish vortical and extensional regions of the flow not only in the 2D NS case but also in 2D MHD, 2D fluid turbulence with polymer additives, and in the 2D HVBK system. The study of turbulence in these systems is inherently interdisciplinary: we have used a variety of methods, from both fluid mechanics and statistical mechanics, to characterize the properties of turbulence in these systems. We hope our overview will stimulate interdisciplinary studies of the challenging problem of turbulence in these rich 2D systems.

Turbulence and spatiotemporal chaos also occur in several other 2D extended dynamical systems. An illustrative list of examples and references includes the 2D Kuramoto-Sivashinsky system,[216] the 2D complex Ginzburg-Landau system,[217] models for 2D excitable media,[218] models for cardiac tissue,[219,220] active-matter turbulence,[221,222] and turbulence in thin elastic plates.[223] An overview of turbulence in these systems must await a comprehensive review of this vast and rapidly developing field.

[1] R. Fjørtoft, "On the changes in the spectral distribution of kinetic energy for twodimensional, nondivergent flow," Tellus **5**, 225 (1953).

[2] R. H. Kraichnan, "Inertial ranges in two dimensional turbulence," Phys. Fluids **10**, 1417 (1967); Inertial-range transfer in two- and three-dimensional turbulence, J. Fluid Mech. **47** 525–535 (1971).

[3] C. Leith, "Diffusion approximation for two-dimensional turbulence," Phys. Fluids **11**, 671 (1968).

[4] G. K. Batchelor, "Computation of the energy spectrum in homogeneous two-dimensional turbulence," Phys. Fluids **12**, II-233 (1969).

[5] U. Frisch, *Turbulence the Legacy of A. N. Kolmogorov* (Cambridge University Press, Cambridge, 1996).

[6] M. Lesieur, *Turbulence in Fluids*, Fluid Mechanics and Its Applications Vol. 84 (Springer, The Netherlands, 2008).

[7] G. Boffetta and R. E. Ecke, "Two-dimensional turbulence," Annu. Rev. Fluid Mech. **44**, 427–451 (2012).

[8] R. Pandit, P. Perlekar, and S. S. Ray, "Statistical properties of turbulence: An overview," Pramana **73**, 157 (2009).

[9] J. Charney, "Geostrophic turbulence," J. Atmos. Sci. **28**, 1087–1095 (1971).

[10] P. B. Rhines, "Geostrophic turbulence," Annu. Rev. Fluid Mech. **11**, 401 (1979).

[11] R. Salmon, *Lectures on Geophysical Fluid Dynamics* (Oxford University Press, NY, 1998).

[12] F. Bouchet and A. Venaille, "Statistical mechanics of two-dimensional and geophysical flows," Phys. Rep. **515**, 227–295 (2012).

[13] K. S. Gage, "Evidence for a $k^{5/3}$ law inertial range in mesoscale two-dimensional turbulence," J. Atmos. Sci. **36**(10), 1950–1954 (1979).

[14] K. S. Gage and G. D. Nastrom, "Theoretical interpretation of atmospheric wavenumber spectra of wind and temperature observed by commercial aircraft during GASP," J. Atmos. Sci. **43**(7), 729–740 (1986).

[15] D. K. Lilly, "Two-dimensional turbulence generated by energy sources at two scales," J. Atmos. Sci. **46**(13), 2026–2030 (1989).

[16] R. Tulloch and K. S. Smith, "A theory for the atmospheric energy spectrum: Depth-limited temperature anomalies at the tropopause," Proc. Natl. Acad. Sci. U. S. A. **103**(40), 14690–14694 (2006).

[17] P. L. Read, "Transition to geostrophic turbulence in the laboratory, and as a paradigm in atmospheres and oceans," Surv. Geophys. **22**(3), 265–317 (2001).

[18] B. Galperin, H. Nakano, H.-P. Huang, and S. Sukoriansky, "The ubiquitous zonal jets in the atmospheres of giant planets and earths oceans," Geophys. Res. Lett. **31**(13), L13303, doi:10.1029/2004gl019691 (2004).

[19] R. B. Scott and B. K. Arbic, "Spectral energy fluxes in geostrophic turbulence: Implications for ocean energetics," J. Phys. Oceanogr. **37**(3), 673–688 (2007).

[20] R. K. Scott and L. M. Polvani, "Forced-dissipative shallow-water turbulence on the sphere and the atmospheric circulation of the giant planets," J. Atmos. Sci. **64**(9), 3158–3176 (2007).

[21] S. A. Balbus and J. F. Hawley, "Instability, turbulence, and enhanced transport in accretion disks," Rev. Mod. Phys. **70**, 1–53 (1998).

[22] B. Mukhopadhyay, N. Afshordi, and R. Narayan, "Bypass to turbulence in hydrodynamic accretion disks: An eigenvalue approach," Astrophys. J. **629**, 383–396 (2005).

[23] A. Brandenburg and A. Nordlund, "Astrophysical turbulence modeling," Rep. Prog. Phys. **74**, 046901 (2011).

[24] J. Sommeria, "Experimental study of the two-dimensional inverse energy cascade in a square box," J. Fluid Mech. **170**, 139–168 (1986).

[25] Y. Couder, J. Chomaz, and M. Rabaud, "On the hydrodynamics of soap films," Phys. D **37**, 384–405 (1989).

[26] M. Gharib and P. Derango, "A liquid film (soap film) tunnel to study two-dimensional laminar and turbulent shear flows," Phys. D **37**, 406–416 (1989).

[27] J. Paret and P. Tabeling, "Experimental observation of the two-dimensional inverse energy cascade," Phys. Rev. Lett. **79**, 4162–4165 (1997).

[28] J. Paret, D. Marteau, O. Paireau, and P. Tabeling, "Are flows electromagnetically forced in thin stratified layers two dimensional?," Phys. Fluids **9**, 3102–3104 (1997).

[29] J. Paret and P. Tabeling, "Intermittency in the two-dimensional inverse cascade of energy: Experimental observations," Phys. Fluids **10**, 3126–3136 (1998).

[30] J. Paret, M. Jullien, and P. Tabeling, "Vorticity statistics in the two-dimensional enstrophy cascade," Phys. Rev. Lett. **83**, 3418–3421 (1999).

[31] J. M. Chomaz, "The dynamics of a viscous soap film with soluble surfactant," J. Fluid Mech. **442**, 387–409 (2001).

[32] M. A. Rutgers, "Forced 2D turbulence: Experimental evidence of simultaneous inverse energy and forward enstrophy cascades," Phys. Rev. Lett. **81**, 2244–2247 (1998).

[33] M. Rivera, P. Vorobieff, and R. E. Ecke, "Turbulence in flowing soap films: Velocity, vorticity, and thickness fields," Phys. Rev. Lett. **81**, 1417–1420 (1998).

[34] M. Rivera and X. L. Wu, "External dissipation in driven two-dimensional turbulence," Phys. Rev. Lett. **85**, 976–979 (2000).

[35] M. Rivera, X. L. Wu, and C. Yeung, "Universal distribution of centers and saddles in two-dimensional turbulence," Phys. Rev. Lett. **87**, 044501 (2001).

[36] M. Rivera and X. L. Wu, "Homogeneity and the inertial range in driven two-dimensional turbulence," Phys. Fluids **14**, 3098–3108 (2002).

[37] M. Rivera, W. B. Daniel, S. Y. Chen, and R. E. Ecke, "Energy and enstrophy transfer in decaying two-dimensional turbulence," Phys. Rev. Lett. **90**, 104502 (2003).

[38] H. Xia, M. Shats, and G. Falkovich, "Spectrally condensed turbulence in thin layers," Phys. Fluids **21**, 125101 (2009).

[39] N. T. Ouelette, Turbulence in two dimensions, Phys. Today **65**(5), 68 (2012).

[40] N. Francois, H. Xia, H. Punzmann, and M. Shats, "Inverse energy cascade and emergence of large coherent vortices in turbulence driven by Faraday waves," Phys. Rev. Lett. **110**, 194501 (2013).

[41] Y. Liao and N. T. Ouellette, "Geometry of scale-to-scale energy and enstrophy transport in two-dimensional flow," Phys. Fluids **26**, 045103 (2014).

[42] G. E. Moore, "Cramming more components onto integrated circuits," Electronics **38**(8), 114–117 (1965), reprinted in IEEE Solid-State Circuits Society Newsletter **11**(5), 33–35 (2006); see also https://en.wikipedia.org/wiki/Moore's_law.

[43] D. Lilly, "Numerical simulation of two-dimensional turbulence," Phys. Fluids **12**, II-240–II-249 (1969); "Numerical simulation studies of two-dimensional turbulence: I. Models of statistically steady turbulence," Geophys. Fluid Dyn. **3**, 289–319 (1972).

[44] E. D. Siggia and H. Aref, "Point-vortex simulation of the inverse energy cascade in two-dimensional turbulence," Phys. Fluids **24**, 171–173 (1981).

[45] C. Basdevant, B. Legras, R. Sadourny, and M. Beland, "Study of barotropic model flows: Intermittency, waves and predictability," J. Atmos. Sci. **38**, 2305 (1981).

[46] M. Hossain, W. H. Matthaeus, and D. Montgomery, "Long-time states of inverse cascades in the presence of a maximum length scale," J. Plasma Phys. **30**, 479 (1983).

[47] U. Frisch and P. L. Sulem, "Numerical simulation of the inverse cascade in two-dimensional turbulence," Phys. Fluids **27**, 1921–1923 (1984).

[48] L. M. Smith and V. Yakhot, "Bose condensation and small-scale structure generation in a random force driven 2D turbulence," Phys. Rev. Lett. **71**, 352 (1993).

[49] L. M. Smith and V. Yakhot, "Finite-size effects in forced two-dimensional turbulence," J. Fluid Mech. **274**, 115 (1994).

[50] M. Farge, K. Schneider, and N. Kevlahan, "Non-Gaussianity and coherent vortex simulation for two-dimensional turbulence using an adaptive orthogonal wavelet basis," Phys. Fluids **11**, 2187 (1999).

[51] C. V. Tran and J. C. Bowman, "Robustness of the inverse cascade in two-dimensional turbulence," Phys. Rev. E **69**, 036303 (2004).

[52] M. Chertkov, C. Connaughton, I. Kolokolov, and V. Lebedev, "Dynamics of energy condensation in two-dimensional turbulence," Phys. Rev. Lett. **99**, 084501 (2007).

[53] G. Boffetta, "Energy and enstrophy fluxes in the double cascade of two-dimensional turbulence," J. Fluid Mech. **589**, 253–260 (2007).

[54] P. Perlekar and R. Pandit, "Statistically steady turbulence in thin films: Direct numerical simulations with Ekman friction," New J. Phys. **11**, 073003 (2009).

[55] G. Boffetta and S. Musacchio, "Evidence for the double cascade scenario in two-dimensional turbulence," Phys. Rev. E **82**, 016307 (2010).

[56] C.-K. Chan, D. Mitra, and A. Brandenburg, "Dynamics of saturated energy condensation in two-dimensional turbulence," Phys. Rev. E **85**, 036315 (2012).

[57] R. H. Kraichnan and D. Montgomery, "Two-dimensional turbulence," Rep. Prog. Phys. **43**(5), 547 (1980).

[58] P. Tabeling, "Two-dimensional turbulence: A physicist approach," Phys. Rep. **362**(1), 1–62 (2002).

[59] H. Kellay and W. I. Goldburg, "Two-dimensional turbulence: A review of some recent experiments," Rep. Prog. Phys. **65**, 845–894 (2002).

[60] G. van Heijst and H. Clercx, "Laboratory modeling of geophysical vortices," Annu. Rev. Fluid Mech. **41**, 143–164 (2009).

[61] G. Falkovich, "Symmetries of the turbulent state," J. Phys. A: Math. Theor. **42**, 123001 (2009).

[62] H. Tennekes and J. Lumley, *A First Course in Turbulence* (MIT Press, 1972).

[63] D. Biskamp, *Magnetohydrodynamic Turbulence* (Cambridge University Press, Cambridge, 2003).

[64] K. Nam, E. Ott, T. M. Antonsen, and P. N. Guzdar, "Lagrangian chaos and the effect of drag on the enstrophy cascade in two-dimensional turbulence," Phys. Rev. Lett. **84**, 5134 (2000).

[65] G. Boffetta, A. Celani, S. Musacchio, and M. Vergassola, "Intermittency in two-dimensional Ekman-Navier-Stokes turbulence," Phys. Rev. E **66**, 026304 (2002).

[66] G. Boffetta, A. Cenedese, S. Espa, and S. Musacchio, "Effects of friction on 2D turbulence: An experimental study of the direct cascade," Europhys. Lett. **71**, 590–596 (2005).

[67] D. Bernard, G. Boffetta, A. Celani, and G. Falkovich, "Conformal invariance in two-dimensional turbulence," Nat. Phys. **2**, 124–128 (2006); Inverse turbulent cascades and conformally invariant curves," Phys. Rev. Lett. **98**, 024501 (2007).

[68] J. Herault, F. Pétrélis, and S. Fauve, "Experimental observation of 1/f noise in quasi-bidimensional turbulent flows," Europhys. Lett. **111**, 44002 (2015); G. Michel, J. Herault, F. Pétrélis, and S. Fauve, "Bifurcations of a large-scale circulation in a quasi-bidimensional turbulent flow," *ibid.* **115**, 64004 (2016); S. Fauve, J. Herault, G. Michel, and F. Pétrélis, "Instabilities on a turbulent background," J. Stat. Mech.: Theory Exp. **2017**(6), 064001.

[69] P. K. Mishra, J. Herault, S. Fauve, and M. K. Verma, "Dynamics of reversals and condensates in two-dimensional Kolmogorov flows," Phys. Rev. E **91**, 053005 (2015).

[70] V. Shukla, S. Fauve, and M. Brachet, "Statistical theory of reversals in two-dimensional confined turbulent flows," Phys. Rev. E **94**, 061101(R) (2016).

[71] F. Bouchet and E. Simonnet, "Random changes of flow topology in two-dimensional and geophysical turbulence," Phys. Rev. Lett. **102**, 094504 (2009).

[72] J. K. Eaton and J. R. Fessler, "Preferential concentration of particles by turbulence," Int. J. Multiphase Flow **20**, 169–209 (1994).

[73] M. R. Maxey and J. J. Riley, "Equation of motion for a small rigid sphere in a nonuniform flow," Phys. Fluids **26**, 883–889 (1983).

[74] R. Gatignol, "The Faxen formulae for a rigid particle in an unsteady nonuniform Stokes flow," J. Mec. Theor. Appl. **1**, 14360 (1983).

[75] M. Cencini, J. Bec, L. Biferale, G. Boffetta, A. Celani, A. Lanotte, S. Musacchio, and F. Toschi, "Dynamics and statistics of heavy particles in turbulent flows," J. Turbul. **7**, N36 (2006).

[76] F. Toschi and E. Bodenschatz, "Lagrangian properties of particles in turbulence," Annu. Rev. Fluid Mech. **41**, 375 (2009).

[77] J. P. L. C. Salazar and L. R. Collins, "Two-particle dispersion in isotropic turbulent flows," Annu. Rev. Fluid Mech. **41**, 405 (2009).

[78] S. Balachandar and J. K. Eaton, "Turbulent dispersed multiphase flow," Annu. Rev. Fluid Mech. **42**, 111–133 (2010).

[79] A. Babiano, C. Basdevant, P. Le Roy, and R. Sadoumy, "Single-particle dispersion, Lagrangian structures function and Lagrangian energy spectrum in two-dimensional incompressible turbulence," J. Mar. Res. **45**, 107–131 (1987).

[80] A. Babiano, C. Basdevant, P. Le Roy, and R. Sadoumy, "Relative dispersion in two-dimensional turbulence," J. Fluid Mech. **214**, 535–557 (1990).

[81] A. Provenzale, A. Babiano, and B. Villone, "Single-particle trajectories in two-dimensional turbulence," Chaos, Solitons Fractals **5**(10), 2055–2071 (1995).

[82] G. Boffetta and I. M. Sokolov, "Statistics of two-particle dispersion in two-dimensional turbulence," Phys. Fluids **14**, 3224 (2002).

[83] S. Goto and J. C. Vassilicos, "Particle pair diffusion and persistent streamline topology in two-dimensional turbulence," New J. Phys. **6**, 65 (2004).

[84] M. van Aartrijk and H. J. H. Clercx, "Preferential concentration of heavy particles in stably stratified turbulence," Phys. Rev. Lett. **100**, 254501 (2008).

[85] N. T. Ouellette and J. P. Gollub, "Curvature fields, topology, and the dynamics of spatiotemporal chaos," Phys. Rev. Lett. **99**, 194502 (2007).

[86] N. T. Ouellette and J. P. Gollub, "Dynamic topology in spatiotemporal chaos," Phys. Fluids **20**, 064104 (2008).

[87] L. Chen, S. Goto, and J. C. Vassilicos, "Turbulent clustering of stagnation points and inertial particles," J. Fluid Mech. **553**, 143–154 (2006).

[88] G. Boffetta, F. De Lillo, and A. Gamba, "Large scale inhomogeneity of inertial particles in turbulent flow," Phys. Fluids **16**, L20 (2004).

[89] M. Wilczek, O. Kamps, and R. Friedrich, "Lagrangian investigation of two-dimensional decaying turbulence," Phys. D **237**, 2090 (2008).

[90] B. Kadoch, D. del Castillo-Negrete, W. J. T. Bos, and K. Schneider, "Lagrangian statistics and flow topology in forced two-dimensional turbulence," Phys. Rev. E **83**, 036314 (2011).

[91] A. Gupta, D. Mitra, P. Perlekar, and R. Pandit, "Statistical properties of the intrinsic geometry of heavy-particle trajectories in two-dimensional, homogeneous, isotropic turbulence," preprint arXiv:1402.7058 (2014).

[92] A. J. Bray, S. N. Majumdar, and G. Schehr, "Persistence and first-passage properties in nonequilibrium systems," Adv. Phys. **62**, 225 (2013).

[93] P. Perlekar, S. S. Ray, D. Mitra, and R. Pandit, "The persistence problem in two-dimensional fluid turbulence," Phys. Rev. Lett. **106**, 054501 (2011).

[94] V. I. Belinicher and V. S. Lvov, "A scale-invariant theory of fully developed hydrodynamic turbulence," Sov. Phys. JETP **66**, 303 (1987).

[95] V. S. Lvov, E. Podivilov, and I. Procaccia, "Temporal multiscaling in hydrodynamic turbulence," Phys. Rev. E **55**, 7030 (1997).

[96] D. Mitra and R. Pandit, "Varieties of dynamic multiscaling in fluid turbulence," Phys. Rev. Lett. **93**, 024501 (2004).

[97] D. Mitra and R. Pandit, "Dynamics of passive-scalar turbulence," Phys. Rev. Lett. **95**, 144501 (2005).

[98] R. Pandit, S. S. Ray, and D. Mitra, "Dynamic multiscaling in turbulence," Eur. Phys. J. B **64**, 463 (2008).

[99] S. S. Ray, D. Mitra, and R. Pandit, "The universality of dynamic multiscaling in homogeneous, isotropic Navier-Stokes and passive-scalar turbulence," New J. Phys. **10**, 033003 (2008).

[100] S. S. Ray, D. Mitra, P. Perlekar, and R. Pandit, "Dynamic multiscaling in two-dimensional fluid turbulence," Phys. Rev. Lett. **107**, 184503 (2011).

[101] A. Gupta, D. Vincenzi, and R. Pandit, "Elliptical tracers in two-dimensional, homogeneous, isotropic fluid turbulence: The statistics of alignment, rotation, and nematic order," Phys. Rev. E **89**, 021001(R) (2014); G. B. Jeffery, "The motion of ellipsoidal particles immersed in a viscous fluid," Proc. R. Soc. A **102**, 161 (1922).

[102] U. Frisch, A. Pouquet, J. Léorat, and A. Mazure, "Possibility of an inverse cascade of magnetic helicity in magnetohydrodynamic turbulence," J. Fluid Mech. **68**, 769 (1975).

[103] A. Pouquet, "On two-dimensional magnetohydrodynamic turbulence," J. Fluid Mech. **88**, 1 (1978).

[104] J. Sommeria and R. Moreau, "Why, how, and when, MHD turbulence becomes two-dimensional," J. Fluid Mech. **118**, 507 (1982).

[105] D. Biskamp and U. Bremer, "Dynamics and statistics of inverse cascade processes in 2D magnetohydrodynamic turbulence," Phys. Rev. Lett. **72**, 3819 (1994).

[106] R. Kinney, J. C. McWilliams, and T. Tajima, "Coherent structures and turbulent cascades in two-dimensional incompressible magnetohydrodynamic turbulence," Phys. Plasmas **2**, 3623 (1995).

[107] D. Biskamp, E. Schwarz, and A. Celani, "Nonlocal bottleneck effect in two-dimensional turbulence," Phys. Rev. Lett. **81**, 4855 (1998).

[108] D. Biskamp and E. Schwarz, "On two-dimensional magnetohydrodynamic turbulence," Phys. Plasmas **8**, 3282 (2001).

[109] M. K. Verma and V. Eswaran, "Comment on 'On two-dimensional magnetohydrodynamic turbulence' [Phys. Plasmas 8, 3282 (2001)]," Phys. Plasmas **9**, 1484 (2002).

[110] M. K. Verma, "Statistical theory of magnetohydrodynamic turbulence: Recent results," Phys. Rep. **401**, 229–380 (2004).

[111] A. Celani, M. Cencini, A. Mazzino, and M. Vergassola, "Active versus passive scalar turbulence," Phys. Rev. Lett. **89**, 234502 (2002).

[112] A. Celani, M. Cencini, A. Mazzino, and M. Vergassola, "Active and passive fields face to face," New J. Phys. **6**, 72 (2004).

[113] S. Servidio, W. H. Matthaeus, M. A. Shay, P. A. Cassak, and P. Dmitruk, "Magnetic reconnection in two-dimensional magnetohydrodynamic turbulence," Phys. Rev. Lett. **102**, 115003 (2009).

[114] M. Wan, W. H. Matthaeus, S. Servidio, and S. Oughton, "Generation of X-points and secondary islands in 2D magnetohydrodynamic turbulence," Phys. Plasmas **20**, 042307 (2013).

[115] D. Banerjee and R. Pandit, "Statistics of the inverse-cascade regime in two-dimensional magnetohydrodynamic turbulence," Phys. Rev. E **90**, 013018 (2014).

[116] K. Seshasayanan, S. J. Benavides, and A. Alexakis, "On the edge of an inverse cascade," Phys. Rev. E **90**, 051003(R) (2014).

[117] K. Seshasayanan and A. Alexakis, "Critical behavior in the inverse to forward energy transition in two-dimensional magnetohydrodynamic flow," Phys. Rev. E **93**, 013104 (2016).

[118] B. A. Toms, in *Proceedings of the 1st International Congress on Rheology* (North-Holland, Amsterdam, 1949), Vol. II, p. 135; J. Lumley, "Drag reduction in turbulent flow by polymer additives," J. Polym. Sci.: Macromol. Rev. **7**, 263 (1973); P. Virk, "Drag reduction fundamentals," AIChE J. **21**, 625 (1975); W. J. Han, Y. Z. Dong, and H. J. Choi, "Applications of water-soluble polymers in turbulent drag reduction," Processes **5**, 24 (2017).

[119] A. Groisman and V. Steinberg, "Elastic turbulence in a polymer solution flow," Nature **405**, 53 (2000).

[120] R. Ganapathy and A. K. Sood, "Intermittency route to rheochaos in wormlike micelles with flow-concentration coupling," Phys. Rev. Lett. **96**, 108301 (2006).

[121] S. S. Ray and D. Vincenzi, "Elastic turbulence in a shell model of polymer solution," Europhys. Lett. **114**, 44001 (2016).

[122] J. W. Hoyt, "A Freeman scholar lecture: The effect of additives on fluid friction," J. Basic Eng. **94**, 258 (1972).

[123] E. van Doorn, C. M. White, and K. R. Sreenivasan, "The decay of grid turbulence in polymer and surfactant solutions," Phys. Fluids **11**, 2387 (1999).

[124] C. Kalelkar, R. Govindarajan, and R. Pandit, "Drag reduction by polymer additives in decaying turbulence," Phys. Rev. E **72**, 017301 (2005).

[125] P. Perlekar, D. Mitra, and R. Pandit, "Manifestations of drag reduction by polymer additives in decaying, homogeneous, isotropic turbulence," Phys. Rev. Lett. **97**, 264501 (2006).

[126] P. Perlekar, D. Mitra, and R. Pandit, "Direct numerical simulations of statistically steady, homogeneous, isotropic fluid turbulence with polymer additives," Phys. Rev. E **82**, 066313 (2010).

[127] W.-H. Cai, F.-C. Li, and H.-N. Zhang, "DNS study of decaying homogeneous isotropic turbulence with polymer additives," J. Fluid Mech. **665**, 334 (2010).

[128] F. De Lillo, G. Boffetta, and S. Musacchio, "Control of particle clustering in turbulence by polymer additives," Phys. Rev. E **85**, 036308 (2012).

[129] N. Ouellette, H. Xu, and E. Bodenschatz, "Bulk turbulence in dilute polymer solutions," J. Fluid Mech. **629**, 375 (2009).

[130] R. Benzi, E. S. C. Ching, and I. Procaccia, "Drag reduction in homogeneous turbulence by scale-dependent effective viscosity," Phys. Rev. E **70**, 026304 (2004).

[131] R. Benzi, E. S. C. Ching, and C. K. Wong, "Polymer-induced change in scaling behavior in two-dimensional homogeneous turbulent thermal convection," Phys. Rev. E **89**, 053001 (2014).

[132] T. Watanabe and T. Gotoh, "Power-law spectra formed by stretching polymers in decaying isotropic turbulence," Phys. Fluids **26**, 035110 (2014).

[133] Y. Amarouchene and H. Kellay, "Polymers in 2D turbulence: Suppression of large scale fluctuations," Phys. Rev. Lett. **89**, 104502 (2002).

[134] H. Kellay, "Polymers suppress the inverse transfers of energy and the enstrophy flux fluctuations in two-dimensional turbulence," Phys. Rev. E **70**, 036310 (2004).

[135] Y. Jun, J. Zhang, and X.-L. Wu, "Polymer effect on small and large scale two-dimensional turbulece," Phys. Rev. Lett. **96**, 024502 (2006).

[136] G. Boffetta, A. Celani, and S. Musacchio, "Two-dimensional turbulence of dilute polymer solutions," Phys. Rev. Lett. **91**, 034501 (2003); G. Boffetta, A. Celani, and A. Mazzino, "Drag reduction in the turbulent Kolmogorov flow," Phys. Rev. E **71**, 036307 (2005).

[137] S. Berti, A. Bistagnino, G. Boffetta, A. Celani, and S. Musacchio, "Two-dimensional elastic turbulence," Phys. Rev. E **77**, 055306 (2008).

[138] S. Berti and G. Boffetta, "Elastic waves and transition to elastic turbulence in a two-dimensional viscoelastic Kolmogorov flow," Phys. Rev. E **82**, 036314 (2010).

[139] Y. L. Xiong, C. H. Brueneua, and H. Kellay, "Direct numerical simulations of 2D channel flows in the presence of polymers," Europhys. Lett. **95**, 64003 (2011).

[140] A. Gupta, P. Perlekar, and R. Pandit, "Two-dimensional homogeneous isotropic fluid turbulence with polymer additives," Phys. Rev. E **91**, 033013 (2015).

[141] A. Gupta and R. Pandit, "Melting of a nonequilibrium vortex crystal in a fluid film with polymers: Elastic versus fluid turbulence," Phys. Rev. E **95**, 033119 (2017).

[142] E. L. C. M. Plan VI, A. Gupta, D. Vincenzi, and J. D. Gibbon, "Lyapunov dimension of elastic turbulence," J. Fluid Mech. **822**, R4 (2017).

[143] P. M. Chaikin and T. C. Lubensky, *Principles of Condensed Matter Physics*, reprinted ed. (Cambridge University Press, Cambridge, 2000).

[144] M. Kardar, *Statistical Physics of Fields* (Cambridge University Press, UK, 2007).

[145] P. Hohenberg and B. I. Halperin, "Theory of dynamic critical phenomena," Rev. Mod. Phys. **49**, 435 (1977).

[146] J. Lothe and G. M. Pound, "On the statistical mechanics of nucleation theory," J. Chem. Phys **45**, 630 (1966); J. S. Huang, S. Vernon, and N. C. Wong, "Homogeneous nucleation in a critical binary fluid mixture," Phys. Rev. Lett. **33**, 140 (1974).

[147] J. W. Cahn and J. E. Hilliard, "Free energy of a nonuniform system. I. Interfacial free energy," J. Chem. Phys. **28**, 258–267 (1958); J. W. Cahn, "On spinodal decomposition," Acta Metall. **9**, 795 (1961); Spinodal decomposition," Trans. Metall. Soc. AIME **242**, 166 (1968).

[148] J. D. Gunton, M. San Miguel, and P. S. Sahni, "The dynamics of first order phase transitions," in *Phase Transitions and Critical Phenomena*, edited by C. Domb and J. Lebowitz (Academic Press, London, 1983), Vol. 8, p. 269.

[149] A. Onuki, *Phase Transition Dynamics* (Cambridge University Press, UK, 2002).

[150] P. Perlekar, R. Benzi, H. J. H. Clercx, D. R. Nelson, and F. Toschi, "Spinodal decomposition in homogeneous and isotropic turbulence," Phys. Rev. Lett. **112**, 014502 (2014).

[151] I. M. Lifshitz and V. V. Slyozov, "The kinetics of precipitation from supersaturated solid solutions," J. Phys. Chem. Solids **19**, 35 (1961); H. Furukawa, "Effect of inertia on droplet growth in a fluid," Phys. Rev. A **31**, 1103 (1985); E. D. Siggia, "Late stages of spinodal decomposition in binary mixtures," *ibid.* **20**, 595 (1979).

[152] A. J. Bray, "Theory of phase ordering kinetics," Adv. Phys. **43**, 357 (1994).

[153] V. M. Kendon, M. E. Cates, I. P. Barraga, J. C. Desplat, and P. Blandon, "Inertial effects in three-dimensional spinodal decomposition of a symmetric binary fluid mixture: A lattice Boltzmann study," J. Fluid Mech. **440**, 147 (2001).

[154] S. Puri, in *Kinetics of Phase Transitions*, edited by S. Puri and V. Wadhawan (CRC Press, Boca Raton, US, 2009), Vol. 6, p. 437.

[155] N. Pal, P. Perlekar, A. Gupta, and R. Pandit, "Binary-fluid turbulence: Signatures of multifractal droplet dynamics and dissipation reduction," Phys. Rev. E **93**, 063115 (2016).

[156] P. Perlekar, N. Pal, and R. Pandit, "Two-dimensional turbulence in symmetric binary-fluid mixtures: Coarsening arrest by the inverse cascade," Sci. Rep. **7**, 44589 (2017).

[157] X. Fan, P. H. Diamond, L. Chacón, and H. Li, "Cascades and spectra of a turbulent spinodal decomposition in two-dimensional symmetric binary liquid mixtures," Phys. Rev. Fluids **1**, 054403 (2016).

[158] R. J. Donnelly, *Quantized Vortices in Helium II* (Cambridge University Press, Cambridge, 1991).

[159] M. Tsubota, "Quantum turbulencefrom superfluid helium to atomic Bose-Einstein condensates," J. Phys.: Condens. Matter **21**, 164207 (2009).

[160] M. S. Paoletti and D. P. Lathrop, "Quantum turbulence," Annu. Rev. Condens. Matter Phys. **2**, 213 (2011).

[161] L. Skrbek and K. R. Sreenivasan, "Developed quantum turbulence and its decay," Phys. Fluids **24**, 011301 (2012).

[162] N. G. Berloff, M. Brachet, and N. P. Proukakis, "Modeling quantum fluid dynamics at nonzero temperatures," Proc. Natl. Acad. Sci. U. S. A. **111**, 4675 (2014).

[163] R. J. Donnelly, "Cryogenic fluid dynamics," J. Phys.: Condens. Matter **11**, 7783 (1999).

[164] C. F. Barenghi, R. J. Donnelly, and W. F. Vinen, "Friction on quantized vortices in helium II: A review," J. Low Temp. Phys. **52**, 189 (1983).

[165] H. E. Hall and W. F. Vinen, "The rotation of liquid helium II: The theory of mutual friction in uniformly rotating helium II," Proc. R. Soc. A **238**, 215 (1956).

[166] I. M. Khalatnikov, *An Introduction to the Theory of Superfluidity* (W. A. Benjamin, New York, 1965).

[167] P. E. Roche, C. F. Barenghi, and E. Lévêque, "Quantum turbulence at finite temperature: The two-fluids cascade," Europhys. Lett. **87**, 54006 (2009).

[168] V. Shukla, A. Gupta, and R. Pandit, "Homogeneous isotropic superfluid turbulence in two dimensions: Inverse and forward cascades in the Hall-Vinen-Bekharevich-Khalatnikov model," Phys. Rev. B **92**, 104510 (2015).

[169] T.-L. Horng, C.-H. Hsueh, S.-W. Su, Y.-M. Kao, and S.-C. Gou, "Two-dimensional quantum turbulence in a nonuniform Bose-Einstein condensate," Phys. Rev. A **80**, 023618 (2009).

[170] R. Numasato and M. Tsubota, "Possibility of inverse energy cascade in two-dimensional quantum turbulence," J. Low Temp. Phys. **158**(3), 415–421 (2010).

[171] R. Numasato, M. Tsubota, and V. S. L'vov, "Direct energy cascade in two-dimensional compressible quantum turbulence," Phys. Rev. A **81**(6), 063630 (2010).

[172] A. S. Bradley and B. P. Anderson, "Energy spectra of vortex distributions in two-dimensional quantum turbulence," Phys. Rev. X **2**, 041001 (2012).

[173] M. T. Reeves, B. P. Anderson, and A. S. Bradley, "Classical and quantum regimes of two-dimensional turbulence in trapped bose-einstein condensates," Phys. Rev. A **86**, 053621 (2012).

[174] V. Shukla, M. Brachet, and R. Pandit, "Turbulence in the two-dimensional Fourier-truncated Gross-Pitaevskii equation," New J. Phys. **15**(11), 113025 (2013).

[175] H. Salman and D. Maestrini, "Long-range ordering of topological excitations in a two-dimensional superfluid far from equilibrium," Phys. Rev. A **94**, 043642 (2016).

[176] M. T. Reeves, T. P. Billam, B. P. Anderson, and A. S. Bradley, "Inverse energy cascade in forced two-dimensional quantum turbulence," Phys. Rev. Lett. **110**(10), 104501 (2013).

[177] T. P. Billam, M. T. Reeves, and A. S. Bradley, "Spectral energy transport in two-dimensional quantum vortex dynamics," Phys. Rev. A **91**, 023615 (2015).

[178] A. Skaugen and L. Angheluta, "Vortex clustering and universal scaling laws in two-dimensional quantum turbulence," Phys. Rev. E **93**, 032106 (2016).

[179] A. Skaugen and L. Angheluta, "Velocity statistics for nonuniform configurations of point vortices," Phys. Rev. E **93**, 042137 (2016).

[180] X. Yu, T. P. Billam, J. Nian, M. T. Reeves, and A. S. Bradley, "Theory of the vortex- clustering transition in a confined two-dimensional quantum fluid," Phys. Rev. A **94**, 023602 (2016).

[181] G. P. Bewley, M. S. Paoletti, K. R. Sreenivasan, and D. P. Lathrop, "Superfluid helium: Visualization of quantized vortices," Nature **441**, 588 (2006).

[182] A. K. Verma, V. Shukla, A. Bhatnagar, and R. Pandit, "The statistical properties of heavy inertial particles in homogeneous and isotropic superfluid turbulence: Studies based on the three-dimensional Hallvinen-Bekharevich-Khalatnikov model" (unpublished).

[183] V. Shukla, M. Brachet, and R. Pandit, "Sticking transition in a minimal model for the collisions of active particles in quantum fluids," Phys. Rev. A **94**, 041602(R) (2016).

[184] C. Canuto, M. Y. Hussaini, A. Quarteroni, and T. A. Zang, *Spectral Methods in Fluid Dynamics* (Springer-Verlag, Berlin, 1988).

[185] See http://www.fftw.org/ for FFTW Library for computing the discrete Fourier transform.

[186] See http://pencil-code.nordita.org/ for Pencil code: a high-order finite-difference code for compressible MHD.

[187] S. M. Cox and P. C. Matthews, "Exponential time differencing for stiff systems," J. Comput. Phys. **176**, 430 (2002).

[188] A. Okubo, "Horizontal dispersion of floatable particles in the vicinity of velocity singularities such as convergences," Deep-Sea Res. Oceanogr. Abstr. **17**, 445 (1970).

[189] J. Weiss, "The dynamics of enstrophy transfer in two-dimensional hydrodynamics," Phys. D **48**, 273 (1991).

[190] R. B. Bird, R. C. Armstrong, and O. Hassager, *Dynamics of Polymeric Liquids*, 2nd ed. (Wiley, New York, 1987), Vol. 1.

[191] T. Vaithianathan and L. R. Collins, "Numerical approach to simulating turbulent flow of a viscoelastic polymer solution," J. Comput. Phys. **187**, 1 (2003).

[192] D. Vincenzi, P. Perlekar, L. Biferale, and F. Toschi, "Impact of the Peterlin approximation on polymer dynamics in turbulent flows," Phys. Rev. E **92**, 053004 (2015).

[193] A. Celani, A. Mazzino, P. Muratore–Ginanneschi, and L. Vozella, "Phase-field model for the Rayleigh-Taylor instability of immiscible fluids," J. Fluid Mech. **622**, 115–134 (2009).

[194] L. Scarbolo and A. Soldati, "Turbulence modulation across the interface of a large deformable drop," J. Turbul. **14**(11), 27 (2013).

[195] P. Yue, J. J. Feng, C. Liu, and J. Shen, "A diffuse-interface method for simulating two-phase flows of complex fluids," J. Fluid Mech. **515**, 293–317 (2004).

[196] A. Gupta and M. Sbragaglia, "Deformation and breakup of viscoelastic droplets in confined shear flow," Phys. Rev. E **90**, 023305 (2014).

[197] J. D. Gibbon, N. Pal, A. Gupta, and R. Pandit, "Regularity criterion for solutions of the three-dimensional Cahn-Hilliard-Navier-Stokes equations and associated computations," Phys. Rev. E **94** 063103 (2016).

[198] N. Pal, Ph.D. thesis, Indian Institute of Science, 2017; N. Pal, P. Perlekar, S. S. Ray, A. Gupta, and R. Pandit, "Droplets in laminar flows and statistically homogeneous turbulence: From many droplets to a few droplets in the Cahn-Hilliard-Navier-Stokes equations" (unpublished).

[199] See http://www.nvidia.com/object/cuda_home_new.html for Cuda: for general computing on graphical processing units (GPUs).

[200] P. Perlekar, L. Biferale, M. Sbragaglia, S. Srivastava, and F. Toschi, "Droplet size distribution in homogeneous isotropic turbulence," Phys. Fluids **24**, 065101 (2012).

[201] R. J. Donnelly and C. F. Barenghi, "The observed properties of liquid helium at the saturated vapor pressure," J. Phys. Chem. Ref. Data **27**, 1217 (1998).

[202] S. Nazarenko and M. Onorato, "Freely decaying turbulence and Bose-Einstein condensation in Gross-Pitaevski model," J. Low Temp. Phys. **146**, 31–46 (2007).

[203] H. Xu, A. Pumir, G. Falkovich, E. Bodenschatz, M. Shats, H. Xia, N. Francois, and G. Boffetta, "Flight-crash events in turbulence," Proc. Natl. Acad. Sci. U. S. A. **111**, 7558 (2014).

[204] E. Piretto, S. Musacchio, F. De Lillo, and G. Boffetta, "Irreversibility of the two-dimensional enstrophy cascade," Phys. Rev. E **94**, 053116 (2016).

[205] L. Biferale, E. Calzavarini, and F. Toschi, "Multi-time multi-scale correlation functions in hydrodynamic turbulence," Phys. Fluids **23**, 085107 (2011).

[206] A. Bhatnagar, A. Gupta, D. Mitra, R. Pandit, and P. Perlekar, "How long do particles spend in vortical regions in turbulent flows?," Phys. Rev. E **94**, 053119 (2016).

[207] U. Frisch, S. Kurien, R. Pandit, W. Pauls, S. S. Ray, A. Wirth, and J.-Z. Zhu, "Hyperviscosity Galerkin truncation, and bottlenecks in turbulence," Phys. Rev. Lett. **101**, 144501 (2008).

[208] G. Sahoo, P. Perlekar, and R. Pandit, "Systematics of the magnetic-Prandtl-number dependence of homogeneous, isotropic magnetohydrodynamic turbulence," New J. Phys. **13**, 013036 (2011).

[209] W. H. Matthaeus, A. Pouquet, P. D. Mininni, P. Dmitruk, and B. Breech, "Rapid alignment of velocity and magnetic field in magnetohydrodynamic turbulence," Phys. Rev. Lett. **100**, 085003 (2008).

[210] P. Perlekar and R. Pandit, "Turbulence-induced melting of a nonequilibrium vortex crystal in a forced thin fluid film," New J. Phys. **12**, 023033 (2010).

[211] T. V. Ramakrishnan and M. Yussouff, "First-principles order-parameter theory of freezing," Phys. Rev. B **19**, 2775 (1979).

[212] C. Cichowlas, P. Bonȧti, F. Debbasch, and M. Brachet, "Effective dissipation and turbulence in spectrally truncated Euler flows," Phys. Rev. Lett. **95**, 264502 (2005).

[213] S. S. Ray, U. Frisch, S. Nazarenko, and T. Matsumoto, "Resonance phenomenon for the Galerkin-truncated Burgers and Euler equations," Phys. Rev. E **84**, 016301 (2011); A. J. Majda and I. Timofeyev, "Remarkable statistical behavior for truncated Burgers-Hopf dynamics," Proc. Natl. Acad. Sci. U. S. A. **97**, 12413 (2000); D. Banerjee and S. S. Ray, "Transition from dissipative to conservative dynamics in equations of hydrodynamics," Phys. Rev. E **90**, 041001(R) (2014); S. S. Ray, "Thermalized solutions, statistical mechanics and turbulence: An overview of some recent results," Pramana **84**, 395, (2015); D. Venkataraman and S. S. Ray, "The onset of thermalisation in finite-dimensional equations of hydrodynamic: Insights from the Burgers equation," Proc. R. Soc. A **473**, 20160585 (2017).

[214] G. Krstulovic and M. Brachet, "Energy cascade with small-scale thermalization, counterflow metastability and anomalous velocity of vortex rings in Fourier-truncated Gross-Pitaevskii equation," Phys. Rev. E **83**, 066311 (2011).

[215] T. W. Neely, A. S. Bradley, E. C. Samson, S. J. Rooney, E. M. Wright, K. J. H. Law, R. Carretero-González, P. G. Kevrekidis, M. J. Davis, and B. P. Anderson, "Characteristics of two-dimensional quantum turbulence in a compressible superfluid," Phys. Rev. Lett. **111**, 235301 (2013).

[216] C. Jayaprakash, F. Hayot, and R. Pandit, "Universal properties of the two-dimensional Kuramoto-Sivashinsky equation," Phys. Rev. Lett. **71**, 12 (1993); A. Kalogirou, E. E. Keaveny, and D. T. Papageorgiou, "An in-depth numerical study of the two-dimensional Kuramoto-Sivashinsky equation," Proc. R. Soc. A **471**, 20140932 (2015).

[217] G. Grinstein, C. Jayaprakash, and R. Pandit, "Conjectures about phase turbulence in the complex Ginzburg-Landau equation," Phys. D **90**, 96 (1996); H. Chaté and P. Manneville, "Phase diagram of the two-dimensional complex Ginzburg-Landau equation," Phys. A **224**, 348–368 (1996).

[218] A. Pande and R. Pandit, "Spatiotemporal chaos and nonequilibrium transitions in a model excitable medium," Phys. Rev. E **61**, 6448 (2000); M. Bär and M. Eiswirth, "Turbulence due to spiral breakup in a continuous excitable medium," *ibid.* **48**, R1635 (1993); J. Lechleiter, S. Girard, E. Peralta, and D. Clapham, "Spiral calcium wave propagation and annihilation in Xenopus laevis oocytes," Science **252**, 123 (1991).

[219] T. K. Shajahan, A. R. Nayak, and R. Pandit, "Spiral-wave turbulence and its control in the presence of inhomogeneities in four mathematical models of cardiac tissue," PLoS One **4**(3), e4738 (2009).

[220] K. V. Rajany, A. Gupta, A. V. Panfilov, and R. Pandit, "The statistical properties of spiral-and scroll-wave turbulence in cardiac tissue," preprint arXiv:1705.09935 (2017).

[221] J. Dunkel, S. Heidenreich, K. Drescher, H. H. Wensink, M. Bär, and R. E. Goldstein, "Fluid dynamics of bacterial turbulence," Phys. Rev. Lett. **110**, 228102 (2013); S. Ramaswamy, "The mechanics and statistics of active matter," Annu. Rev. Condens. Matter Phys. **1**, 323–345 (2010).

[222] A. Choudhary, D. Venkataraman, and S. S. Ray, "Effect of inertia on model flocks in a turbulent environment," Europhys. Lett. **112**, 24005 (2015).

[223] G. Düring, C. Josserand, S. Rica, "Wave turbulence theory of elastic plates," Phys. D **347**, 42–73 (2017); G. Düring and G. Krstulovic "An exact result in strong wave turbulence of thin elastic plates," e-print arXiv:1703.06159.